[redacted]

ORNL-1215

530

AEC RESEARCH AND DEVELOPMENT REPORT

HEAT TRANSFER AND PRESSURE LOSS IN TUBE BUNDLES FOR HIGH PERFORMANCE HEAT EXCHANGERS AND FUEL ELEMENTS

BY

G. H. Cohen
A. P. Fraas
M. E. LaVerne

OAK RIDGE NATIONAL LABORATORY
OPERATED BY
CARBIDE AND CARBON CHEMICALS COMPANY
A DIVISION OF UNION CARBIDE AND CARBON CORPORATION
OAK RIDGE, TENNESSEE

[redacted]

[redacted]

Index No. ORNL-1215
This document contains 75 pages.
This is copy 53 of 148, Series A.

Subject Category: Reactors-Research and Power

HEAT TRANSFER AND PRESSURE LOSS IN TUBE BUNDLES FOR HIGH PERFORMANCE HEAT EXCHANGERS AND FUEL ELEMENTS

G. H. Cohen*
A. P. Fraas
M. E. LaVerne

August 12, 1952

[redacted]

OAK RIDGE NATIONAL LABORATORY
Operated by
CARBIDE AND CARBON CHEMICALS COMPANY
A DIVISION OF UNION CARBIDE AND CARBON CORPORATION
Oak Ridge, Tennessee

Contract No. W-7405-eng-26

*Formerly with ORNL, presently employed by AEC Lockland Area Office

[redacted]

[redacted]

Index No. ORNL-1215
Reactors-Research and Power

Distribution, Series [redacted]

1-25.	Carbide and Carbon Chemicals Company
26-36.	Argonne National Laboratory
37.	~~Armed Forces Special Weapons Project~~ (Sandia)
38-45.	~~Atomic Energy Commission, Washington~~
46.	~~Battelle Memorial Institute~~
47-49.	~~Brookhaven National Laboratory~~
50.	Bureau of Ships
51-52.	California Research and Development Company
53-64.	Carbide and Carbon Chemicals Company (ORNL)
65.	Chicago Patent Group
66.	~~Chief of Naval~~ Research
67-71.	~~duPont Company~~
72-74.	General Electric Company (ANPP)
75-78.	General Electric Company, Richland
79.	Hanford Operations Office
80-86.	Idaho Operations Office
87.	Iowa State College
88-91.	Knolls Atomic Power Laboratory
92-94.	Los Alamos
95.	Massachusetts Institute of Technology (Kaufmann)
96.	Massachusetts Institute of Technology (Benedict)
97-99.	Mound Laboratory
100-101.	National Advisory Committee for Aeronautics, Cleveland
102.	National Advisory Committee for Aeronautics, Washington
103-104.	New York Operations Office
105-106.	North American Aviation, Inc.
107.	Nuclear Development Associates (NDA)
108.	Patent Branch, Washington
109.	Rand Corporation
110.	Savannah River Operations Office (Augusta)
111.	Savannah River Operations Office (Wilmington)
112-113.	University of California Radiation Laboratory
114.	Vitro Corporation of America
115-118.	Westinghouse Electric Corporation
119-133.	Wright Air Development Center
134-148.	Technical Information Service, Oak Ridge

Carbide and Carbon Chemicals Company internal distribution as follows:

1.	~~C. E. Center~~	10.	M. E. LaVerne
2.	~~C. E. Larson~~	11.	R. N. Lyon
3.	~~L. B. Emlet~~	12.	W. D. Manly
4.	~~W. B. Humes~~	13.	H. F. Poppendiek
5.	A. M. Weinberg	14.	M. Pugacz
6.	E. D. Shipley	15.	H. W. Savage
7.	E. S. Bettis	16.	R. W. Schroeder
8.	R. C. Briant	17.	G. H. Cohen
9.	~~A. P. Fraas~~	18-21.	ANP Reports Office
		~~22-25.~~	Reports Office, TID

~~Issuing Office~~
~~Technical Information Department, Y-12 Plant~~
Date Issued: ~~OCT 4 1952~~

[redacted]

[redacted]

INDEX

[redacted]

[redacted]

LIST OF TABLES

[redacted]

[redacted]

LIST OF ILLUSTRATIONS

[redacted]

[redacted]

LIST OF ILLUSTRATIONS (Continued)

[redacted]

[redacted]

LIST OF ILLUSTRATIONS (Continued)

[redacted]

[redacted]

LIST OF APPENDICES

[redacted]

[redacted]

HEAT TRANSFER AND PRESSURE LOSS IN TUBE BUNDLES FOR HIGH PERFORMANCE HEAT EXCHANGERS AND FUEL ELEMENTS

INTRODUCTION

The bulk and weight of both NEPA and ORNL cross-flow and tube-and-shell heat exchangers of conventional design have made it clear that such designs leave much to be desired and are completely unsuited to the unit shield. A much more promising type of construction for both heat exchangers and fuel elements involves parallel flow through bundles of closely-spaced tubes. However, the problems involved in spacing long slender tubes and in handling the cross-flow regions at the ends had apparently seemed so difficult that nothing had been done with this type of construction until the work covered by this report was initiated.

The writers can find no flow or heat transfer test data in the literature for parallel flow between large numbers of closely-spaced tubes. Because fluid pressure drop, with its attendant fluid pressure forces on the core structure, is a major limitation on the design of high-performance heat exchangers and fuel elements, design data for this geometry are badly needed.

A series of model tests, planned to give the more important pressure drop and heat transfer information required for ANP Program design work, was outlined after considerable discussion by H. F. Poppendiek, H. C. Claiborne, J. H. Wyld, S. V. Manson, and A. P. Fraas. It was decided that two heat exchanger models and three ARE type fuel element bundles should be flow tested with water or air and the heat transfer characteristics of one heat exchanger model should be determined with sodium.

The tube arrangement covered in this report was proposed in June, 1950, as a means of halving the weight and volume required for the heat exchanger. Ideally, the pressure drop across this arrangement should be little more than that required to overcome the skin friction on the tube surfaces. If the pressure drops across the tube spacers and in the cross-flow regions can be kept low, this ideal can be approached. Much of the test work covered in this report was devoted to this phase of the problem.

DESCRIPTION OF MODELS

First Heat Exchanger Airflow Model

The first heat exchanger model was designed as a representative section through the proposed type of full-scale aircraft heat exchanger, a schematic longitudinal cross-section of which is shown in Figure 1. A

[redacted]

three quarter view of the mock-up from the cross-flow end is shown in Figure 2.1. The size of the model, twenty tubes high by twelve tubes wide, was felt to give as small a number of tubes as would constitute a representative section. In order to simplify construction and flow testing, the model was built to be tested with air up to a Reynolds' number of about 10,000.

Because the flow testing involved only flow around the tubes and not through them, the "tubes" were actually made from 1/8-inch diameter solid copper welding rods bent to shape in jigs and assembled in the arrangement shown. Details of the tube shapes, as seen from the cross-flow end, are shown in Figure 2.2. Note that half the tubes have a plane 90^{o} bend while the other half also have an offset, in a plane perpendicular to the first bend, equal to the tube spacing in the parallel-flow section. Arrangement of the two types of bent tube in alternate rows and use of a header plate drilled as shown in Figure 2.2 allows the cross-flow region to be opened up to provide more than ample entrance area to the parallel-flow section of the tube bundle. This construction has the further advantage that the holes in the header plate can be spread apart to virtually any spacing required for easy welding or for strengthening of the header plate. In addition, because of the bends at the ends of the tubes, differential thermal expansion between the tubes and the shell presents no problem.

Tube spacing in the parallel-flow section of the tube bundle was maintained with spacers made from 0.040-inch diameter copper wire that had been flattened to a thickness of 0.020 inch. The horizontal and vertical sets of spacers, shown protruding from the tube bundle in Figure 2.1, were well separated in order to reduce the obstruction to flow around the tubes. After the picture in Figure 2.1 was taken, the ends of the spacers were trimmed off and the sides and top of the model clamped on in order to house the tube matrix and force the tubes and spacers into a compact assembly.

Second Heat Exchanger Airflow Model

Attempts to correlate spacer losses in the first airflow model with spacer and tube dimensions soon led to the firm conviction that more data on a variety of spacers was needed. A second model was therefore built with the primary objective of determining a general correlation of spacer losses with model parameters. The tube matrix consisted of a 10 x 10 bundle of 1/8-inch diameter stainless steel welding rods spaced, as in the first model, by strips of copper wire that had been rolled to the desired thickness. There was no cross-flow region.

Five sets of spacers were prepared; Table I summarizes the pertinent data.

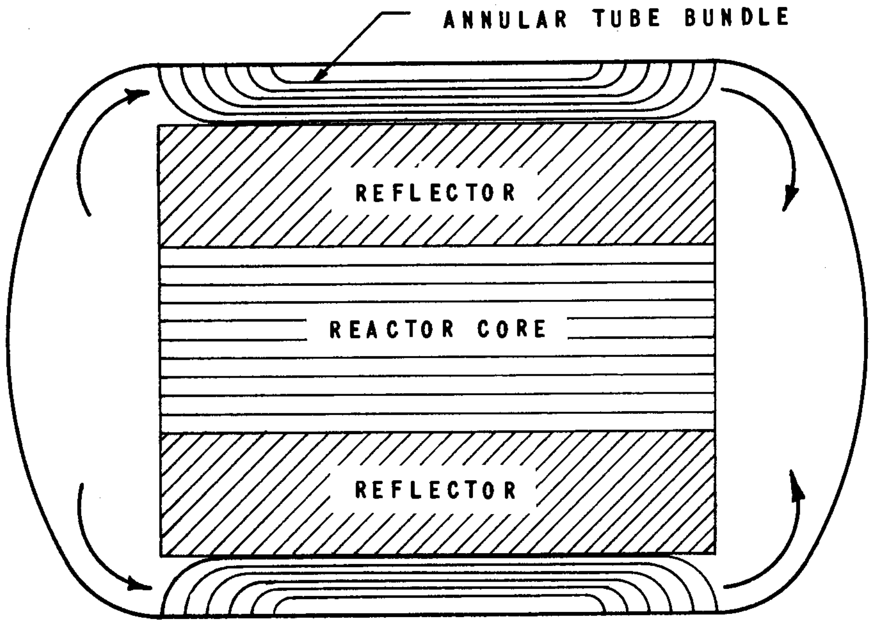

FIGURE NO. 1 - SCHEMATIC LONGITUDINAL CROSS-SECTION THROUGH ANNULAR MODEL OF PROPOSED TYPE OF AIRCRAFT HEAT EXCHANGER.

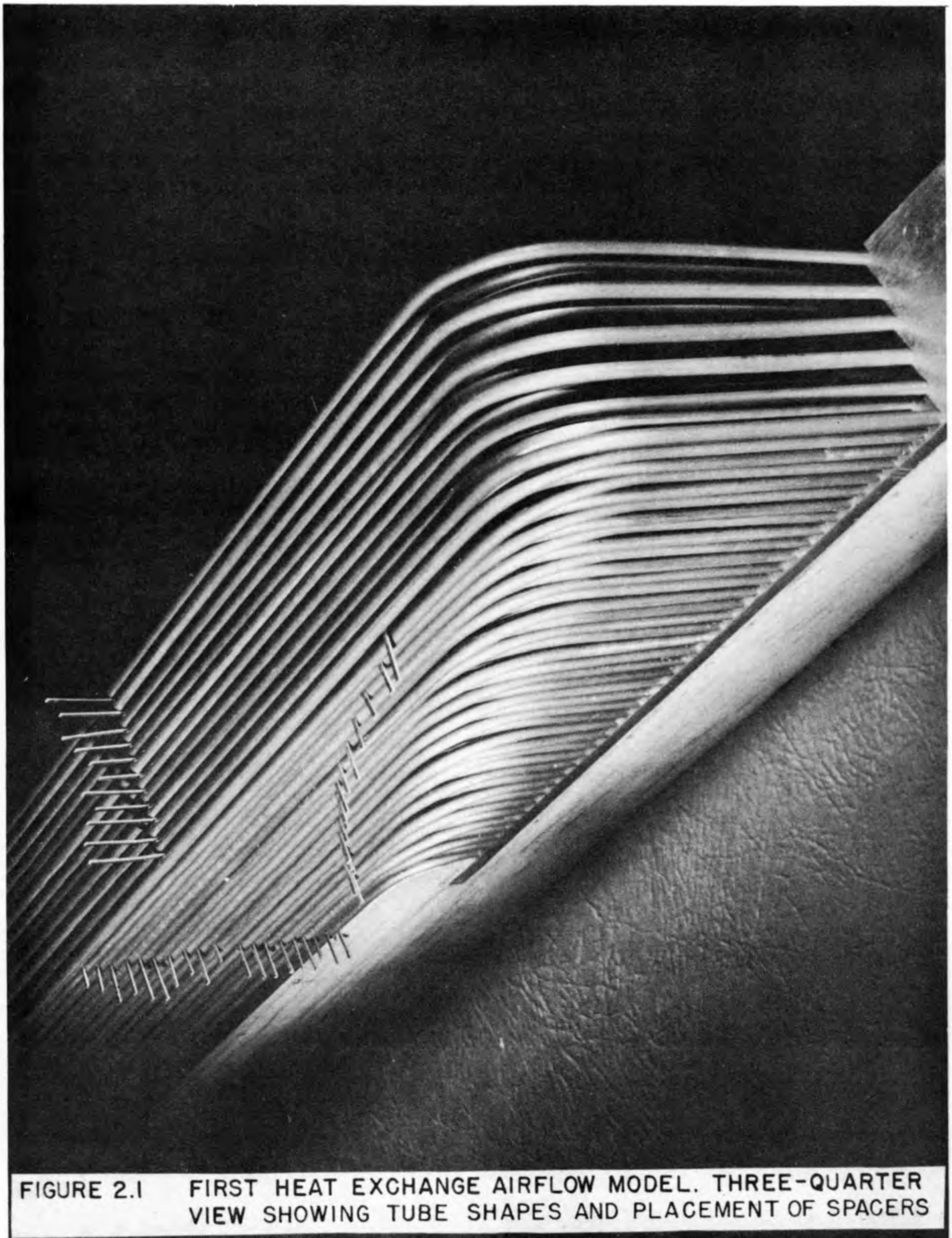

FIGURE 2.1 FIRST HEAT EXCHANGE AIRFLOW MODEL. THREE-QUARTER VIEW SHOWING TUBE SHAPES AND PLACEMENT OF SPACERS

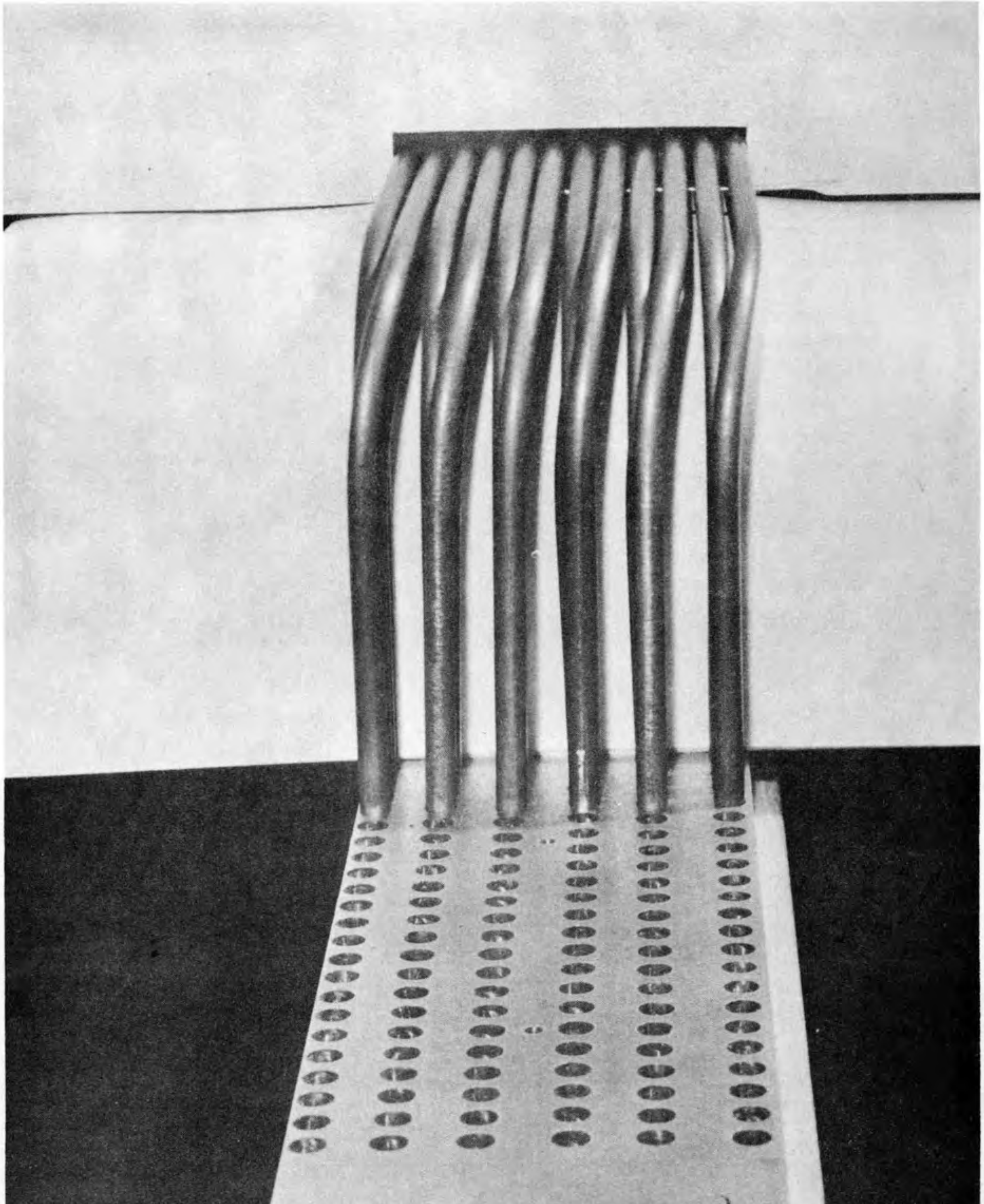

FIGURE 2.2 FIRST HEAT EXCHANGER AIRFLOW MODEL. END VIEW SHOWING DETAILS OF HEADER PLATE AND TUBE SHAPES

Table I

Spacer Data, Second Heat Exchanger Airflow Model

Wire Diameter	Spacer Thickness	Spacer Width	Spacer Thickness / Spacer Width	Spacer Thickness / Tube Diameter
0.040	0.020	0.056	0.358	0.160
0.040	0.032	0.045	0.710	0.256
0.064	0.032	0.088	0.364	0.256
0.102	0.032	0.157	0.204	0.256
0.102	0.051	0.139	0.366	0.408

Spacer and wire dimensions are in inches.

Spacer dimensions were selected to give two groups, the members of each group having a common defining characteristic. Thus, the sets of the first group contained spacers having the same thickness-to-width (approximately 0.36), while the sets of the second group consisted of spacers having the same thickness-to-tube-diameter ratio (approximately 0.26).

Liquid-to-Liquid Heat Exchanger Model

The liquid-to-liquid heat exchanger model was adapted from the first airflow model to give a relatively simple model that could be operated with liquid metal to obtain heat transfer and fluid pressure drop data. Figure 3.1 shows the assembly details of the model. Figures 3.2 and 3.3 show side and end views of the model before the annular jackets were installed around the headers at each end. The tubes were welded into the header at one end by E. S. Bettis using the Bettis-Mann cone-arc process, and Nicrobrazed into the header at the other end by Myron Pugacz at NEPA. Figure 3.4 shows the details of the welded end and Figure 3.5, the brazed end. As in the airflow models, spacers rolled from round wire were used for spacing the tubes in the matrix. A set of 0.020 spacers was placed 1/2 inch from each end of the straight center section and a second set, perpendicular to the first, was installed 2 inches from each end. The welds closing off the holes through which the spacers were inserted can be seen in Figures 3.2, 3.4, and 3.5.

A schematic drawing of the forced circulation loop in which the liquid-to-liquid heat exchanger model was tested is shown in Figure 3.6.

Fuel Element Models

The fuel element models were designed as approximately full scale models of the then extant sodium-cooled ARE fuel element. The basic

					ASSEMBLY USED ON

NO.	MATERIAL	NO. REQ'D	NAME OR DESCRIPTION
1	COR. RES. STL TYPE 347	2	3 3/4 DIA X .120 WALL X 2 7/16 LG. SEAMLESS TUBING
2	"	2	2 5/8 DIA X .083 WALL X 2 1/4 LG. " "
3	"	52	1/8 O.D X .018 WALL X (LENGTH SPECIFIED) SEAMLESS TUBING
4	"	4	3 5/8 DIA X 1/4 THICK
5	"	1	1 1/2 DIA X .083 WALL X 10" LG. - SEAMLESS TUBING.

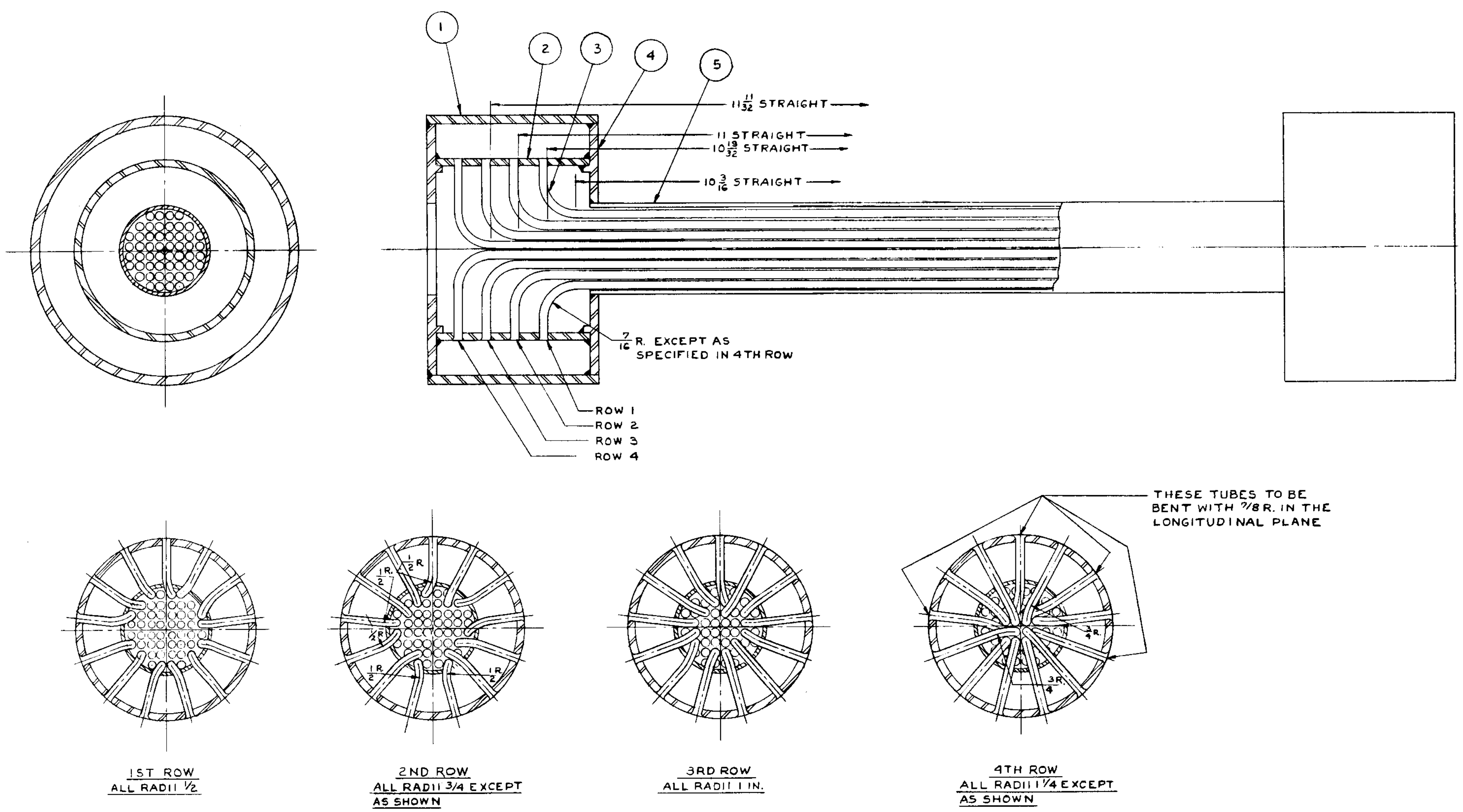

ALL MATERIALS MUST BE DEGREASED BEFORE WELDING.
ALL WELDING TO BE DONE BY THE HELI-ARC PROCESS WITH INERT GAS IN THE PIPE.
ALL HEADER TUBES TO BE WELDED BY THE BETTIS PROCESS.
ALL WELDS MUST BE VACUUM TIGHT AND TESTED.
ALL MATERIAL TO BE STRESS RELIEVED AFTER FORMING FOR 8 HOURS AT 850°F

BREAK ALL SHARP EDGES UNLESS OTHERWISE SPECIFIED
TOLERANCE UNLESS OTHERWISE SPECIFIED — FRACTIONS ± DECIMALS ±

REVISION	BY	DATE	APPROVED FOR OPERATION	DATE	APPROVED FOR DESIGN	DATE			
			PLANT SUPT.		CHIEF ENGR.		DRAWN	R. Weber	3-27-51
			DIV. SUPT.		ENGINEER		TRACED		
			DEPT. SUPT.		SAFETY		CHECKED		
			[illegible signature]	3-76	PLANT PROTECTION		COMP'T'D		
					A. P. Fraas		SCALE FULL SIZE		

CARBIDE AND CARBON CHEMICALS CORPORATION
Y-12 PLANT OAK RIDGE, TENN.

FIGURE 3.1 - LIQUID-TO-LIQUID HEAT EXCHANGER MODEL ASSEMBLY DRAWING

PROJECT	DRAWING NUMBER	REV. LETTER
ANP	DSK-15076	

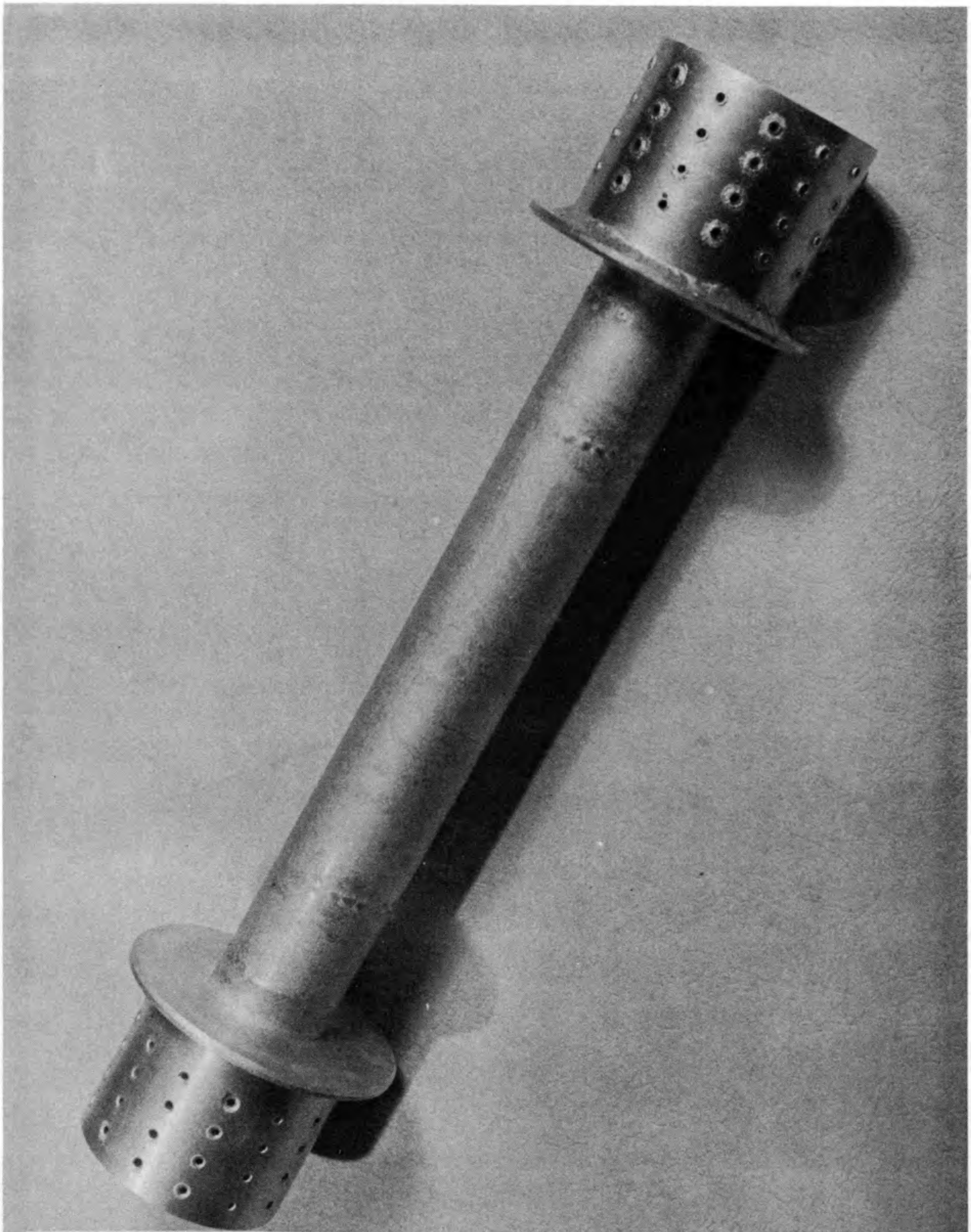

FIGURE 3.2 LIQUID-TO-LIQUID HEAT EXCHANGER MODEL. VIEW SHOWING MODEL COMPLETE EXCEPT FOR ANNULI AND END PLATES

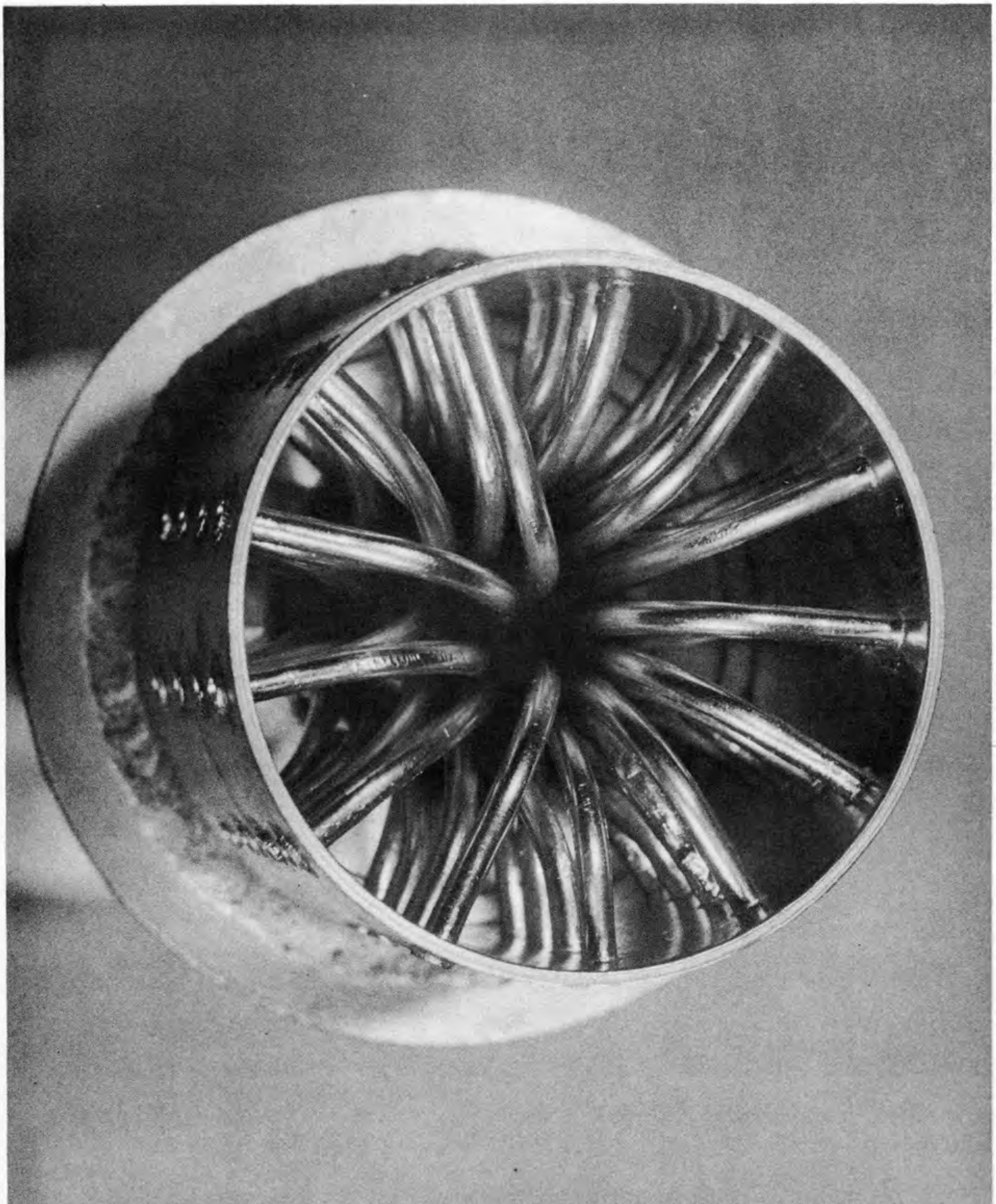

FIGURE 3.3 LIQUID-TO-LIQUID HEAT EXCHANGER MODEL. END VIEW SHOWING DETAILS OF CROSS FLOW REGION

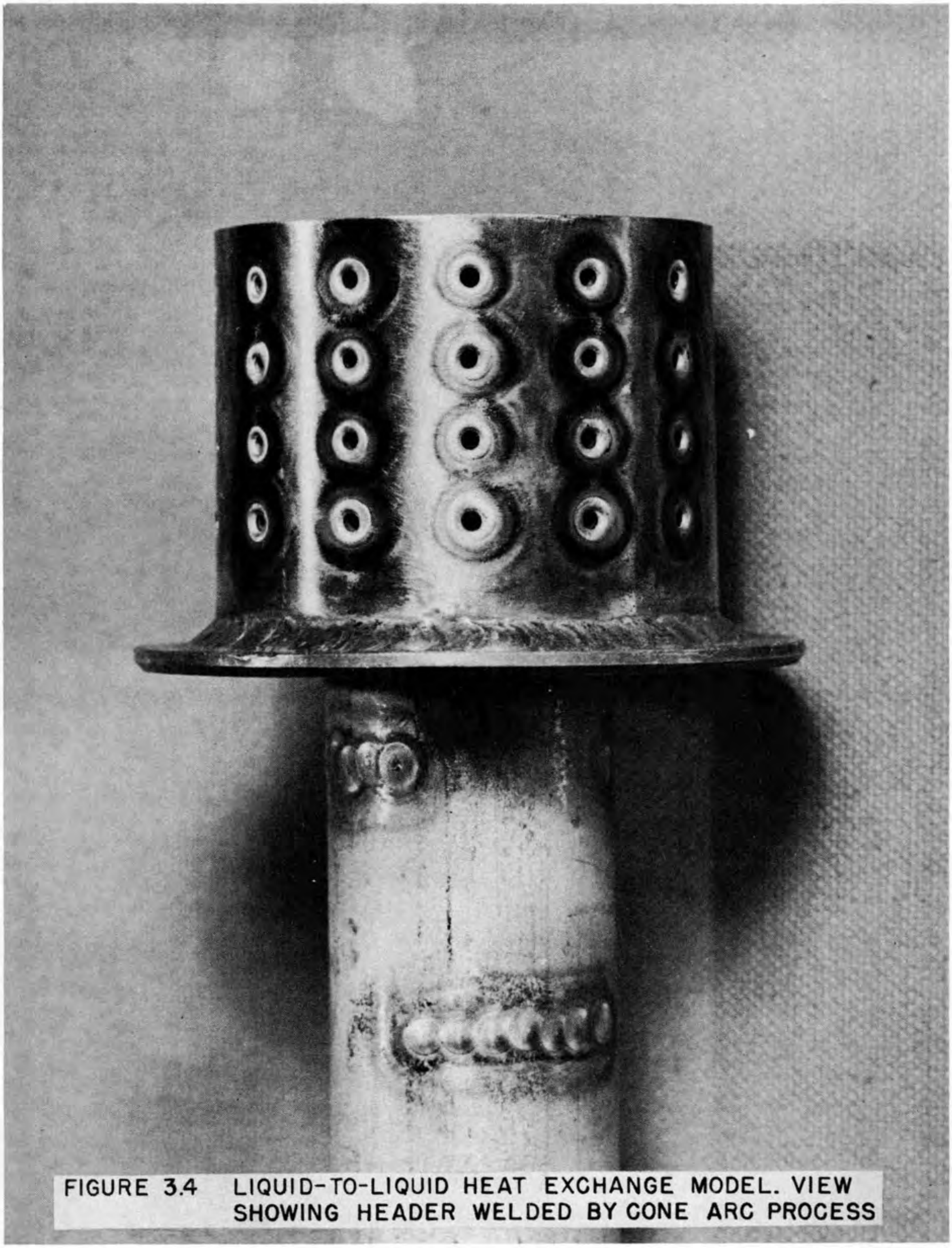

FIGURE 3.4 LIQUID-TO-LIQUID HEAT EXCHANGE MODEL. VIEW SHOWING HEADER WELDED BY CONE ARC PROCESS

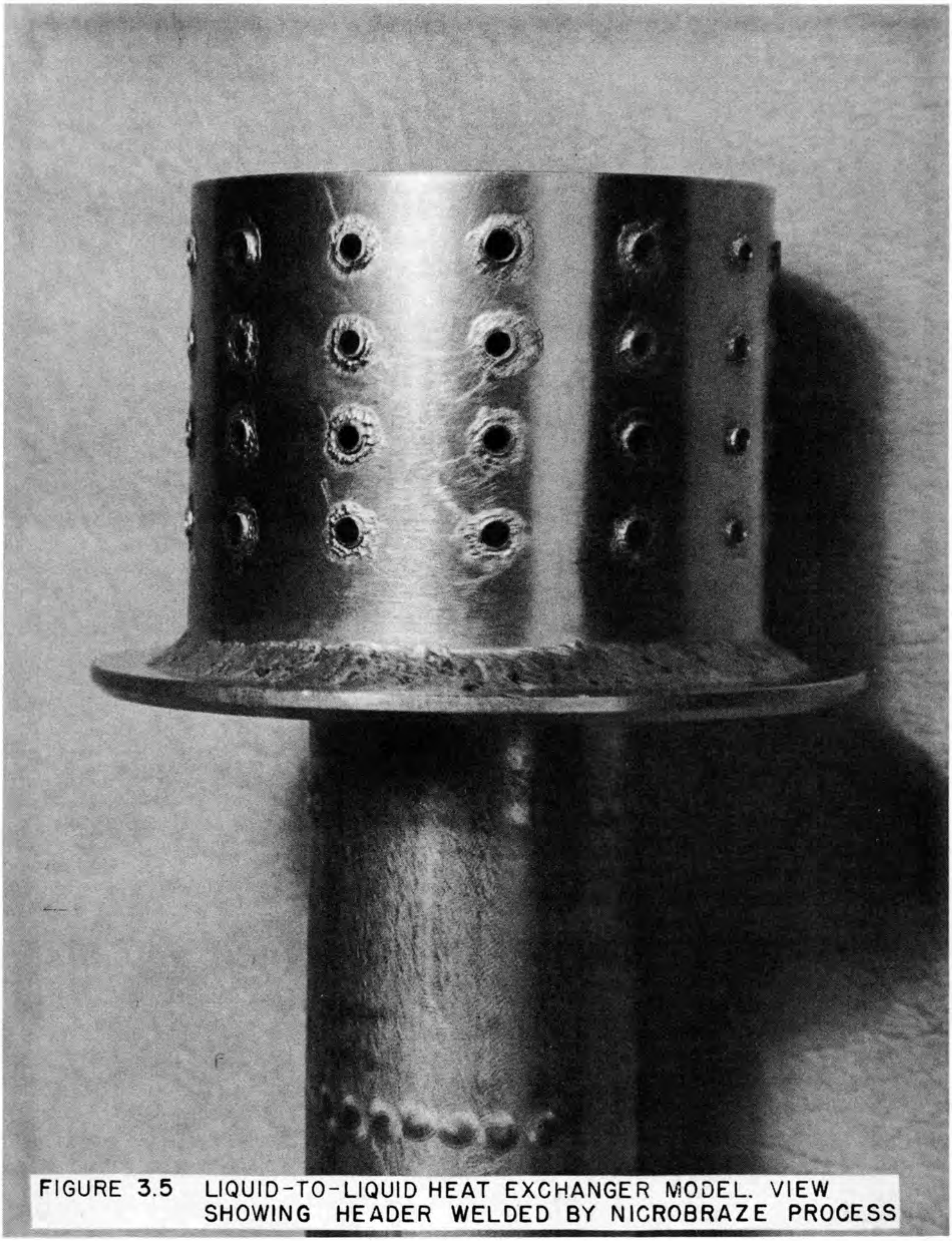

FIGURE 3.5 LIQUID-TO-LIQUID HEAT EXCHANGER MODEL. VIEW SHOWING HEADER WELDED BY NICROBRAZE PROCESS

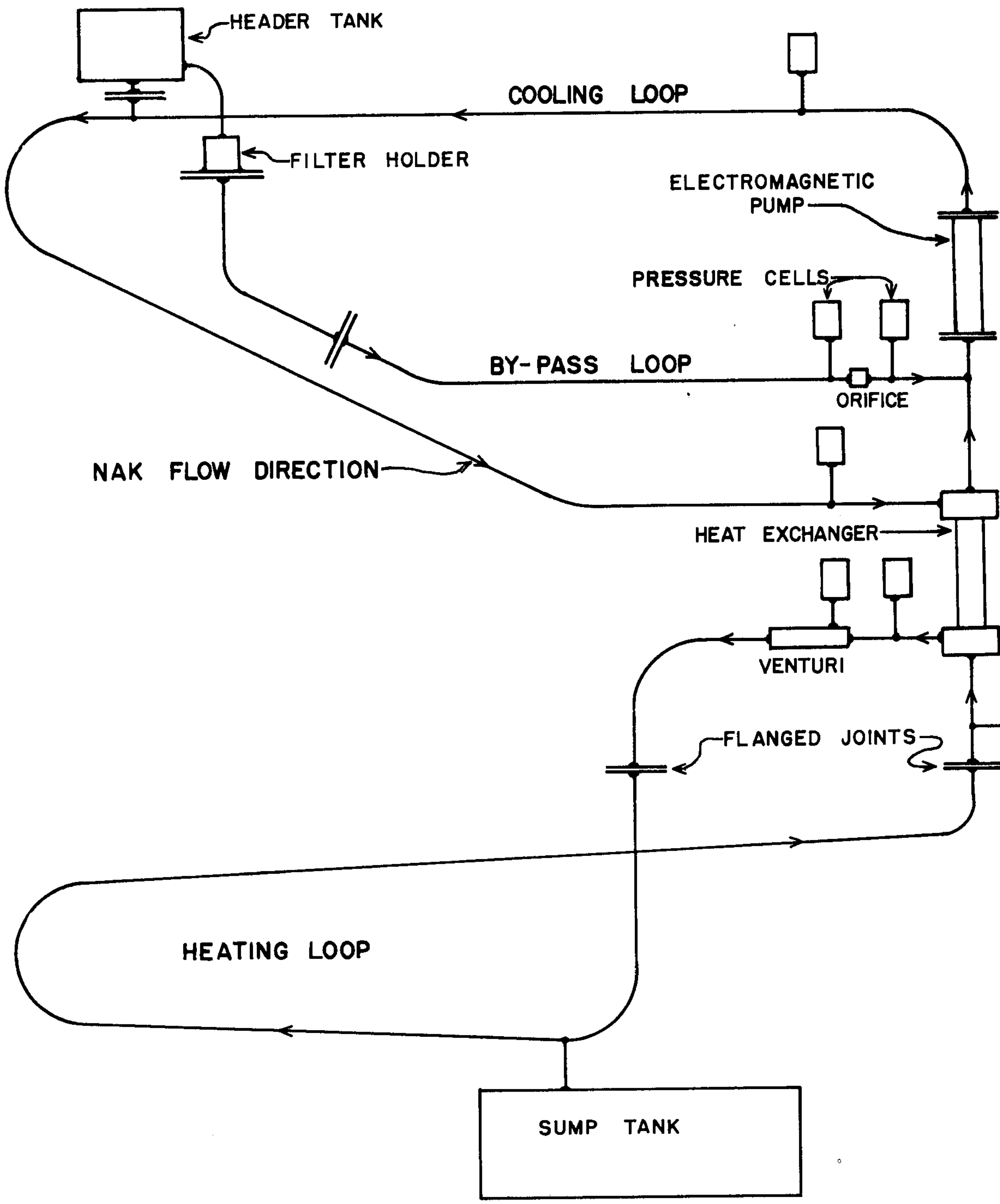

FIGURE NO. 3.6 - LIQUID-TO-LIQUID HEAT EXCHANGER MODEL. SCHEMATIC DRAWING OF FORCED CIRCULATION LOOP USED FOR HEAT TRANSFER AND FLOW TESTS WITH NAK.

model consisted of six hexagonally disposed 4-foot long brass tubes, simulating fuel tubes, inserted in a 4-foot long, 1.105 inch inside diameter, glass tube, simulating a coolant tube, and held in place by various spacers. Figure 4.1 shows a side view of the three tube bundles tested. The cylindrical objects near the ends of two of the three tube bundles are the jigs used in brazing the center spacers. Because only one set of end spacers was available when the photograph was taken, the jigs were used to support the otherwise unsupported tube bundle ends. The center spacers were sections of an 11/16 inch diameter, 0.020 inch thick cylinder, 1/4 inch long, brazed in place with a 0.020 inch fillet. Radial lugs, 0.020 inch thick, were brazed to alternate tubes. Figure 4.2 shows the end spacers used on all the models. The machine screws appearing in the photograph were used for attaching the spacers to the fuel tubes.

Fuel tube diameter and intermediate spacer type were the only differences in the models tested, the same glass tube, type of center spacer, and set of end spacers being used for each test. Fuel tube diameters used were 1/8, 3/16, and 1/4 inch. Three types of tube spacer, in addition to the end and center spacers common to all the models, were also flow tested; Figure 4.3 shows these spacers.

Two spacers of a given type were used for each test. Spacers A were placed approximately midway between the center and ends of the tube bundle. In order to maintain spacers B in position without soldering, it was necessary to place them at the ends of the fuel tubes. The effect of spacer position on losses was then investigated by obtaining data with spacers C, first in a position about midway between the center and ends of the tubes and then at the tube ends.

All the spacers were made from 0.020 inch thick brass and were 1/4 inch in the direction of flow (this applies to each component of spacer A).

HEAT TRANSFER TESTS

The heat transfer tests were made with the heat exchanger of Figures 3.1 to 3.5 operating in the forced circulation loop of Figure 3.6. Conduct of the tests was quite straightforward; because both circuits of the heat exchanger necessarily have the same flow, a single measurement of flow plus determination of the two inlet and two outlet temperatures suffices to determine the exchanger performance. Flow measurements were made with a calibrated venturi and Bourdon tube gages connected by copper tubing to pressure wells at the venturi. Temperatures were measured with chromel-alumel thermocouples welded to the pipes at the heat exchanger inlets and outlets. The exchanger was heavily lagged to reduce radiation losses and prevent thermocouple error from that source.

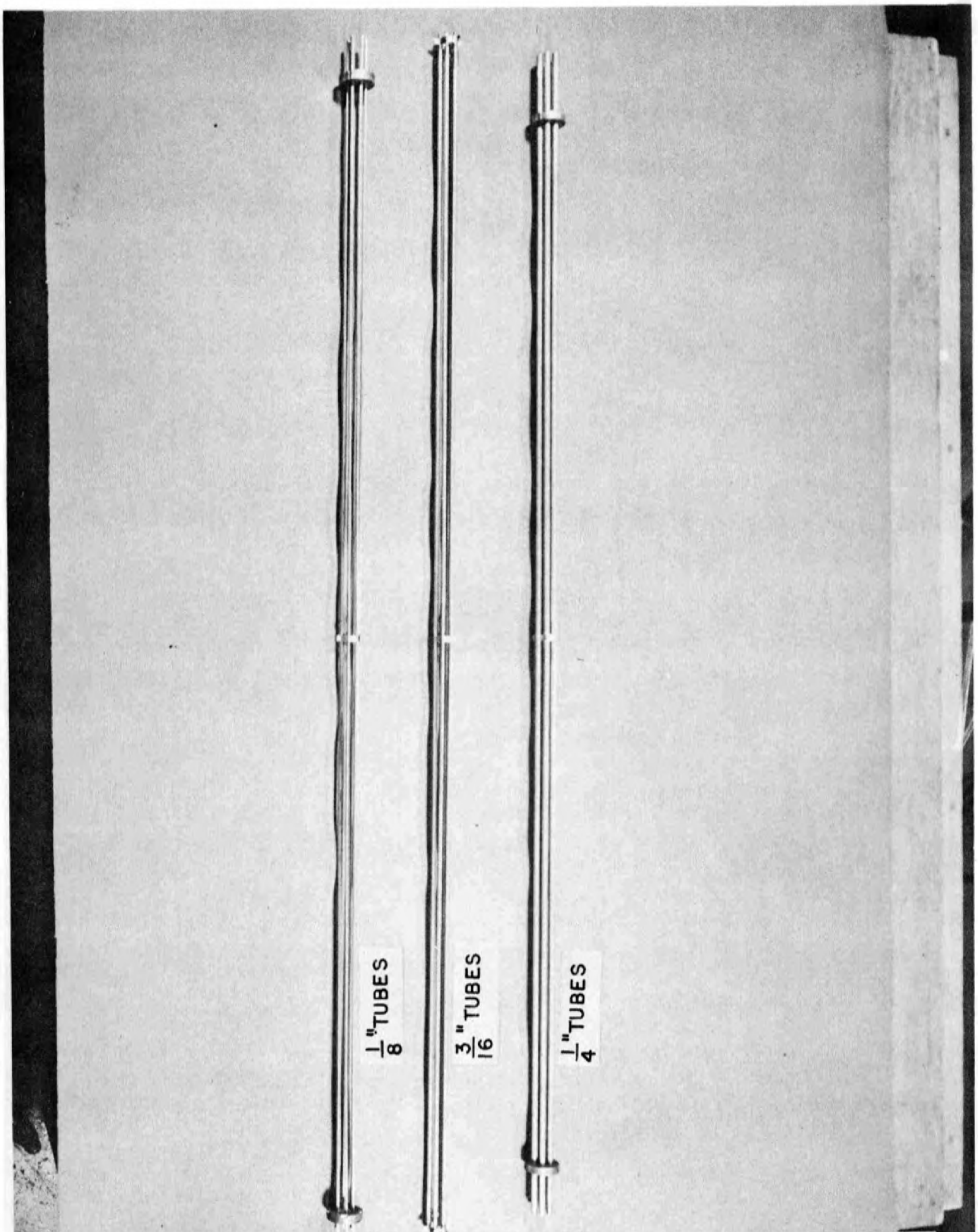

FIGURE 4.1 FUEL ELEMENT MODELS. SIDE VIEW OF THREE TUBE BUNDLES TESTED

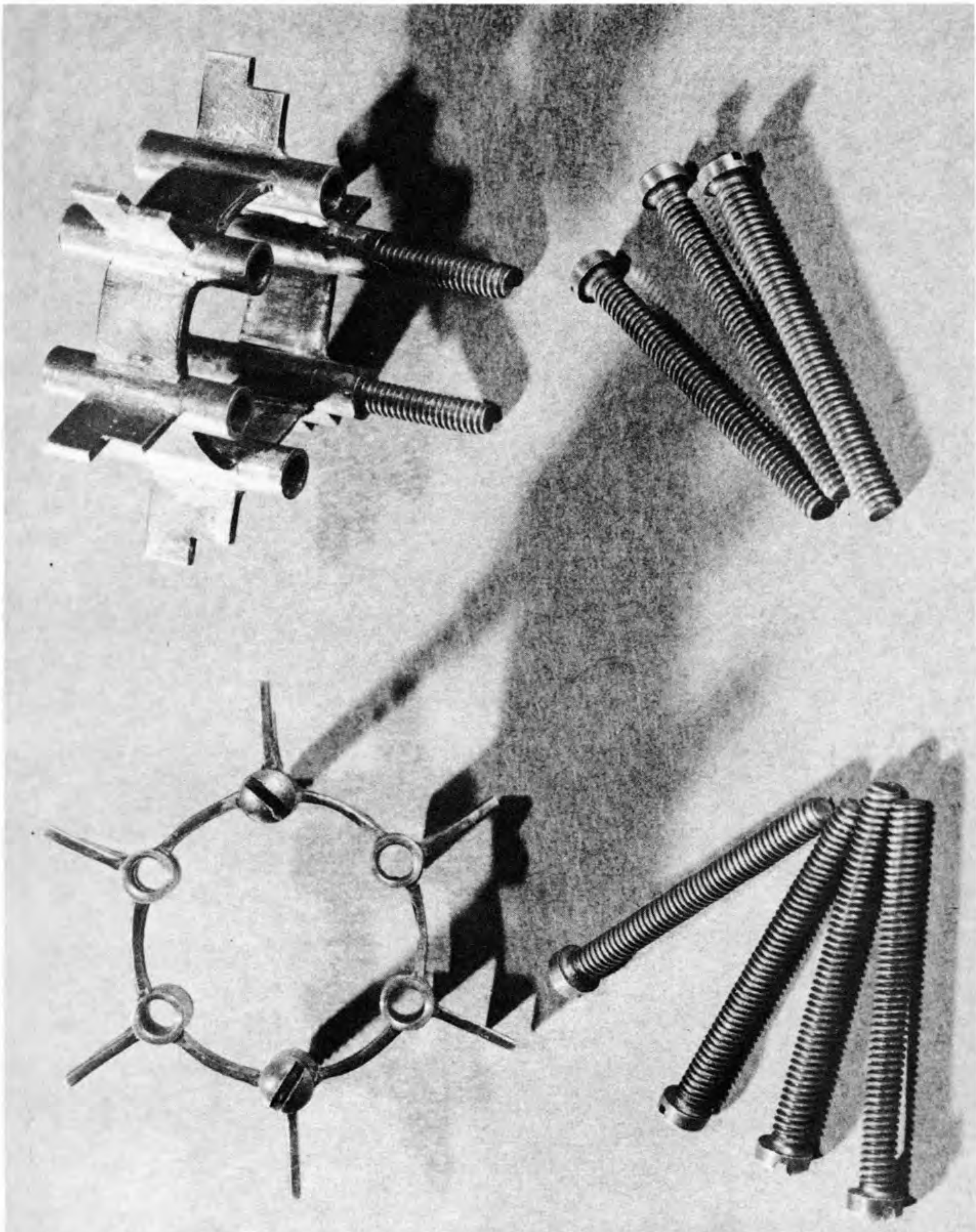

FIGURE 4.2 FUEL ELEMENT MODELS. END SPACERS USED ON ALL MODELS

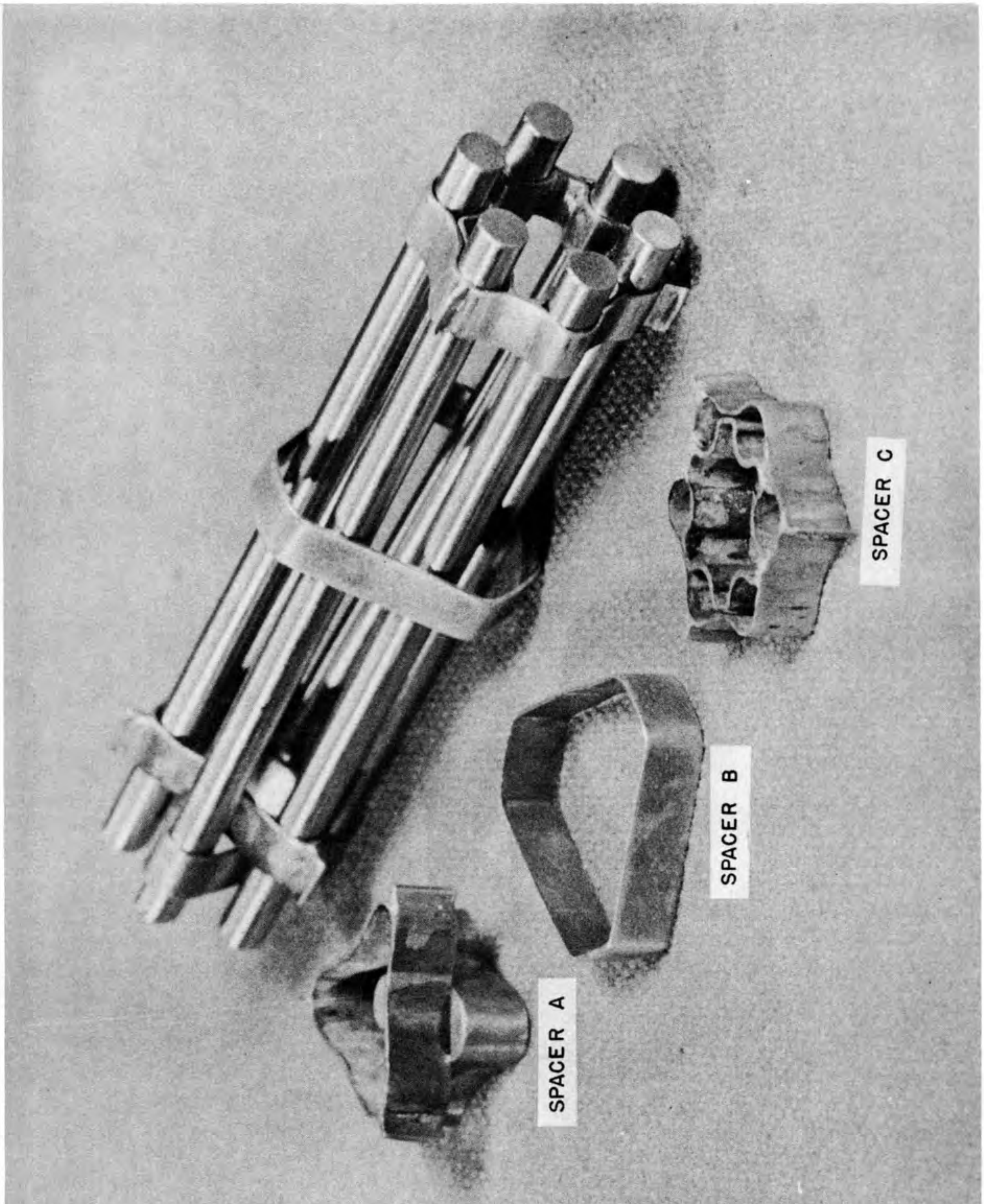

FIGURE 4.3 FUEL ELEMENT MODELS. THREE TUBE-BUNDLE-SPACER TYPES TESTED

In order to insure that, when readings were taken, the system was in a steady state (and yet not unduly protract an already slow process) the following procedure was adopted. The temperature control was set for the exchanger inlet temperature desired; when the temperature recorder indicated the system had steadied out, a complete set of data was taken, followed shortly by a second reading. If the agreement between the two sets of data was sufficiently good (indicative of steady operation), a third and final set of data was taken after a short further wait. In case the first data were taken prematurely, extra sets of data were obtained until good agreement was found.

FLOW TESTS

First Heat Exchanger Airflow Model

The initial flow testing was planned to give information on pressure losses in parallel flow through bundles of closely packed tubes and across tube spacers. The Reynolds' number range extended from approximately 200, well within the laminar flow region, to about 10,000, well into turbulent flow. Later testing covered investigation of pressure losses and distributions in the cross-flow region of the model.

A series of pressure taps was provided along the top and bottom of the model for measurement of pressure drops and pressures. Pressure differences in the model were measured with water manometers, gage pressures being determined by a U-tube mercury manometer with one leg open to atmospheric pressure.

Airflows were measured with a thin-plate orifice upstream of the model. The orifice differential was measured with a U-tube water manometer, while the orifice upstream head was determined by a U-tube mercury manometer having one leg open to atmospheric pressure. Below a Reynolds' number of about 2,000, air was supplied by a centrifugal blower; above that number, the building compressed-air line was used.

Data for determining the friction factor in the tube matrix were obtained by measuring head losses, for a range of airflows, across a three-inch section in the center of a six-inch section of the model containing no spacers. Readings were taken for both top and bottom of the model and averaged to give the loss in the test section.

For determining the incremental losses induced by spacers, head losses for a three-inch section containing a set of horizontal spacers and for one containing a set of vertical spacers were obtained. Averages of the top and bottom readings were used to give the losses in each section. Deduction of the losses in the section without spacers then gave the incremental loss charged to the spacers.

For the cross-flow tests, the air was introduced from the large end of the model. Pressure profiles for both the top and bottom of the model were determined with a multiple-manometer board for a range of airflows. Examination of the data disclosed the existence of a section in the cross-flow region for which there was little or no pressure differential between top and bottom, indicating no transverse flow. Further testing, to higher airflows, was therefore done on that section.

Second Heat Exchanger Airflow Model

Flow testing of this model had as its primary objective a general correlation of spacer losses with spacer and model dimensions, i.e., spacer thickness, spacer width, and tube diameter. Reynolds' numbers attained ranged from about 400 to about 14,000.

A series of taps was provided along the top of the model for measurement of pressures and pressure drops. Spacing of the taps permitted determination of the loss across a short section of the model containing a set of spacers and across clear sections upstream and downstream of the spacer section. The difference in loss between a section containing a set of spacers and a clear section of equal length was then taken to be the increment chargeable to the spacers.

Five series of runs were made, one for each set of spacers. For each series, the model was assembled with one size of spacer and data were taken over as wide a range of airflows as manometer capacity would permit. The head losses in the model were measured with water manometers, absolute head being determined by a U-tube mercury manometer with one leg open to atmospheric pressure.

Airflows were measured with a thin-plate orifice, as in the first heat exchanger model.

Liquid-to-Liquid Heat Exchanger Model

Flow testing of the liquid-to-liquid heat exchanger model consisted of isothermal runs with water and was intended to yield further information on losses in flow through bundles of closely packed tubes and to obtain estimates of end effects.

Friction factor data were obtained by measuring the head loss across a three-inch section of the tube matrix near the center of the heat exchanger. Two 0.025 inch diameter capillary tubes having static pressure holes drilled in their sides were inserted into the matrix with the holes positioned three inches apart. Head differences for a range of water flows were measured with manometers. A rotameter was used for determining flow rates.

In order to get some estimates of end effects, measurements were made of over-all pressure drops around tubes. With the water discharging directly to atmosphere, a single-tube water manometer was used to measure inlet head twenty inches upstream from the heat exchanger. Water flows were again determined with a rotameter.

Fuel Element Models

The water flow tests with the fuel element models provided further checks on the validity of the conventional friction factor correlation when applied to flow through oddly shaped passages such as provided by clusters of tubes. In addition, comparative data were obtained for various tube spacer configuration pressure losses.

Water flows for all the tests were measured with a rotameter. Head losses were determined with a water-mercury U-tube manometer.

Runs were made with the bare coolant tube alone, followed by similar runs with the end spacers of Figure 4.2 added. The 1/8, 3/16, and 1/4 inch tube bundles shown in Figure 4.1 were then successively inserted in the coolant tube with the end spacers and the runs were repeated.

Tests to determine the pressure losses induced by various types of tube spacer were made, using the 3/16 inch tube bundle. The spacers used are shown in Figure 4.3. Two spacers of the same type were placed on the fuel tubes (with end spacers) and the total head loss was found for a range of water flows. The effect of position was investigated by obtaining data with one set of spacers placed first about 11" from the centerline and then near the ends of the tube bundle. It was found necessary to place the triangular spacers near the tube ends to maintain them in position without soldering; the data for this set of spacers is, therefore, for this position only.

RESULTS AND DISCUSSION

Heat Transfer Tests

Two measures of heat transfer were used in determining the performance of the liquid-to-liquid heat exchanger. The first was "cooling effectiveness," η, defined as temperature drop through the exchanger divided by inlet temperature difference, i.e., the number of degrees the hot fluid is cooled per degree of difference between the inlet temperatures of the two streams. The second measure was an "over-all heat transfer coefficient," UA, defined as the heat transferred, in BTU per hour, per degree mean temperature difference between the two streams. An over-all coefficient was used because the difference in area between the inside and outside surfaces of the tubes and the rather large temperature drop through the tube walls (of the same order as that from the tube surfaces to the fluid) precluded calculation of separate coefficients for the two surfaces.

Because flow rates and fluids are the same in the two exchanger circuits, the temperature changes in the two streams should be the same; hence, the two changes were averaged to give the mean temperature drop. Because, in addition, the exchanger operates in pure counterflow, the mean local temperature difference between the two streams should be constant and equal to the difference at either end of the exchanger. These two differences were, therefore, averaged to give the mean temperature difference between the two streams. In an ideal setup the above remarks regarding equality of the two temperature drops and of the two differences would be strictly true; in a real experiment deviations may be expected. The averaging procedure given above was, therefore, followed in order to reduce experimental error.

Cooling effectiveness is given by

$$\eta = \left(1 + \frac{t_4 - t_2}{t_1 - t_3}\right)/2 \tag{1}$$

where t_1 and t_2 are the inlet and outlet temperatures, respectively, of the hotter fluid and t_3 and t_4 are the inlet and outlet temperatures, respectively, of the cooler fluid. Equation (1) was used for computing cooling effectiveness from the experimental data. This form of the expression for η used the average temperature change in the two streams rather than just the drop in the hotter fluid, with a resultant reduction of experimental error in η.

The over-all heat transfer coefficient is given by

$$UA = 105.6\ G\ \frac{\eta}{1 - \eta} \tag{2}$$

where G is the measured flow in gallons per minute. Equation (2) was used to determine the over-all heat transfer coefficient from the experimental data. Averaging was again resorted to in this expression for UA in order to reduce the experimental error.

The symbols used in this report are listed and defined in Appendix A; equations (1) and (2) are derived in Appendix B.

Figure 5.1 presents the parameters η and UA as functions of flow through the heat exchanger in gallons per minute. The experimental points were calculated from equations (1) and (2). The solid curve was calculated from Lyon's equation (ref. 1) for heat transfer coefficient with liquid

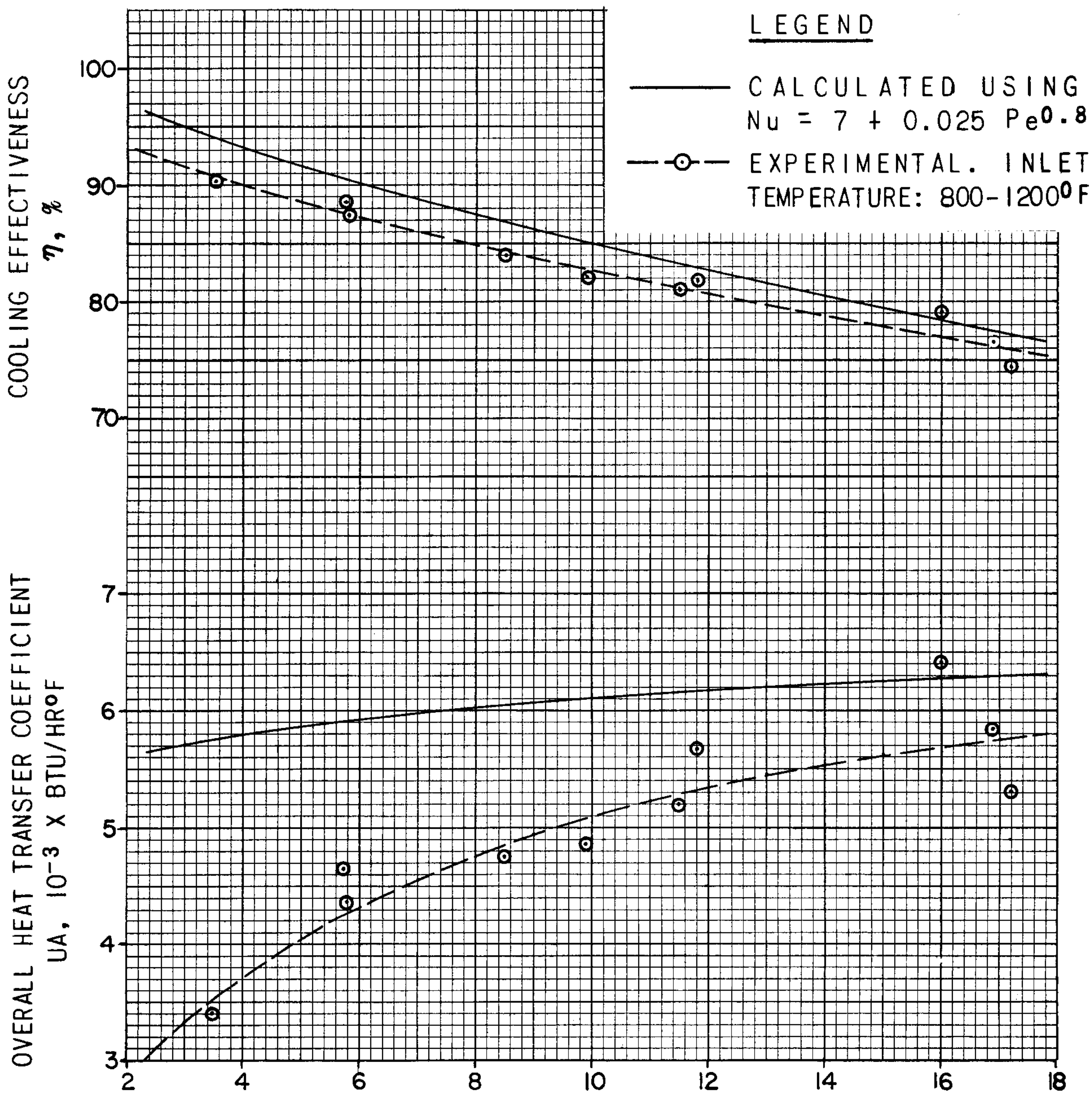

FIGURE NO. 5.1 - LIQUID-TO-LIQUID HEAT EXCHANGER MODEL. COOLING EFFECTIVENESS AND OVER-ALL HEAT TRANSFER COEFFICIENT AGAINST FLOW FOR OPERATION WITH 56% NA - 44% K.

metals,

$$Nu = 7 + 0.025 \, Pe^{0.8}$$

where Nu and Pe are the Nusselt and Peclet numbers for the liquid metal considered.

It is apparent from Figure 5.1 that a discrepancy exists between the experimental results reported here and the computed values. Similar discrepancies of the same order of magnitude have been found by other investigators. It is understood that the NACA recently found what appears to be an error in the basic derivation of the liquid metal heat transfer relation of the preceding paragraph. The revised relation is reported to correlate well with experimental data. See NACA RM E52F05.

Note that the experimental results fall short of the computed by decreasing amounts as the flow is increased. This decrease occurs both in absolute magnitude and percentagewise. Hence, it appears that while the Lyon formula overestimates the heat transfer with liquid metal at low velocities by a considerable margin, the accuracy at higher velocities, i.e., in range of greatest practical interest, should be quite acceptable. The NaK velocity inside the tubes in feet per second happens to be very nearly numerically equal to the flow rate in gallons per minute.

One of the items of considerable concern at the time the heat transfer tests were begun was the question of to what degree the performance of the exchanger would deteriorate with operating time. Figures 5.2 and 5.3 show the effects on performance of endurance running with the exchanger of Figure 3. The exchanger inlet temperature was maintained at 1500°F and the NaK flow at 5.2 gallons per minute throughout the run. No trouble was experienced at any time with the exchanger, the test being voluntarily terminated at 3000 hours.

In Figure 5.2, it will be noticed that the change in over-all heat transfer coefficient with operating time was quite negligible for at least 2000 hours, well within the probable experimental error, in fact. The scatter band enclosing the experimental points may serve to give some notion of the precision of measurement in the tests; the half-width of the band represents the maximum deviation to be expected for a simultaneous 1.5°F error in the four measured temperatures. The over-all heat transfer coefficient was used here because it is a more sensitive indicator of changes in performance than the cooling effectiveness.

Figure 5.3 shows pressure drops both through and around tubes as a function of exchanger operating time. No trend in either set of pressure drop data is apparent at any time during the run, the points scattering

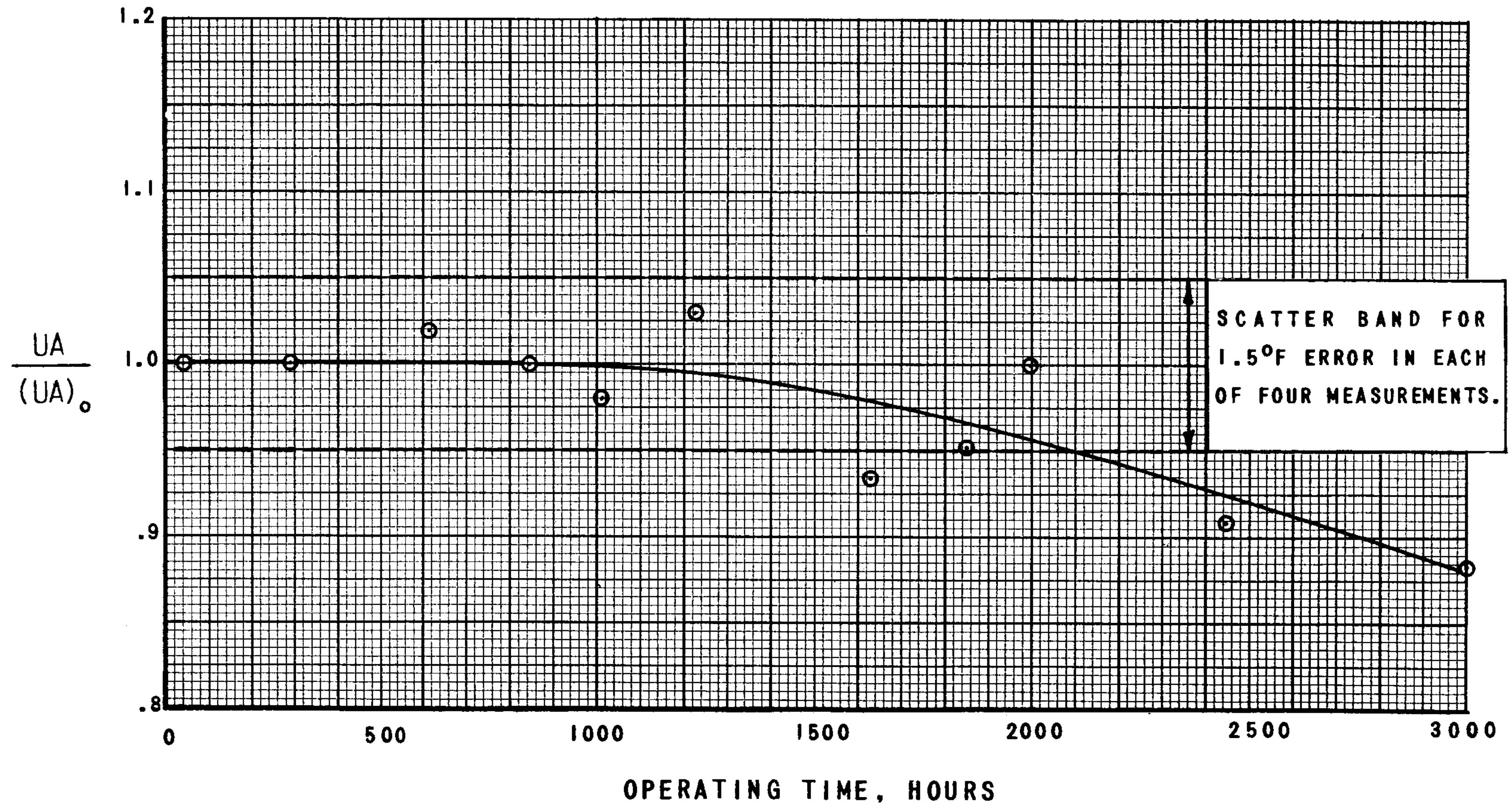

FIGURE NO. 5.2 - LIQUID-TO-LIQUID HEAT EXCHANGER MODEL. EFFECT OF OPERATING TIME ON OVER-ALL HEAT TRANSFER COEFFICIENT.

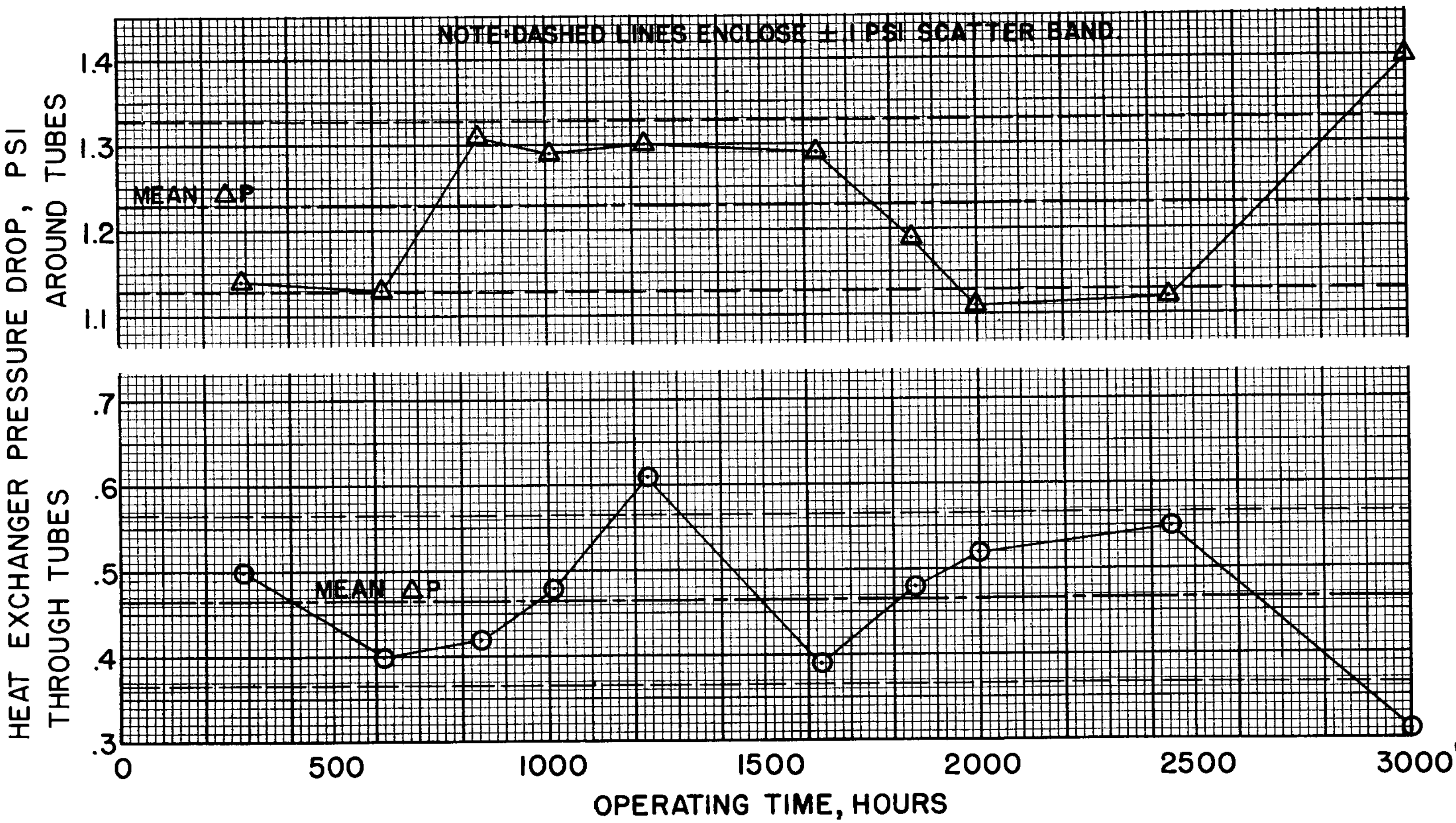

FIGURE NO. 5.3 - LIQUID-TO-LIQUID HEAT EXCHANGER MODEL. EFFECT OF OPERATING TIME ON PRESSURE DROP.

quite randomly about their respective means. Note also that changes in the two pressure drops appear uncorrelated. It would appear, therefore, that the observed loss in performance is chargeable to the formation of a relatively thin film on some of the tube surface rather than to any appreciable clogging of the flow passages. The scatter bands shown represent the maximum deviation for a reading error of 0.05 psi on each of two gauges (the minimum error attainable from careful gauge readings).

Flow Tests

Cross-Flow Tests

Pressure profiles for both top and bottom of the first heat exchanger airflow model over a range of airflows are presented in Figure 6.1. Note that ahead of the corner at the entrance to the parallel-flow region the pressure variations for both surfaces are nearly linear. In the region before the corner, the gradient for the upper surface (where the flow is across the tubes in a fairly open space) is substantially lower than that for the lower surface (where the flow is parallel to the tubes in a more restricted section). There is a very abrupt increase in the upper surface gradient as the flow accelerates around the corner and enters the parallel-flow section. Some effect of the corner is also felt at the lower surface as evidenced by an increase in the pressure gradient there.

For each airflow, there is a point where the two pressure profiles intersect (the "isobaric point") and the upper and lower surface pressures are equal. At the isobaric point the flow has no transverse component. From an examination of the data, it appeared that the section between pressure taps 2 and 3 most nearly approached this desired condition of flow perpendicular to the tubes in the cross-flow region. Data for the cross-flow friction factor determination were therefore taken in that section.

Grimison (ref. 2) presents the results of a correlation of a large amount of data on flow across banks of tubes in the form of a cross-flow friction factor and Reynolds' number parametric with longitudinal and transverse tube spacing and tube outside diameter. His expressions may be written as

$$f_c = \frac{\Delta H}{4N \frac{V^2}{2g}} \tag{3}$$

and

$$N_R = \frac{V D_t w}{\mu} \tag{4}$$

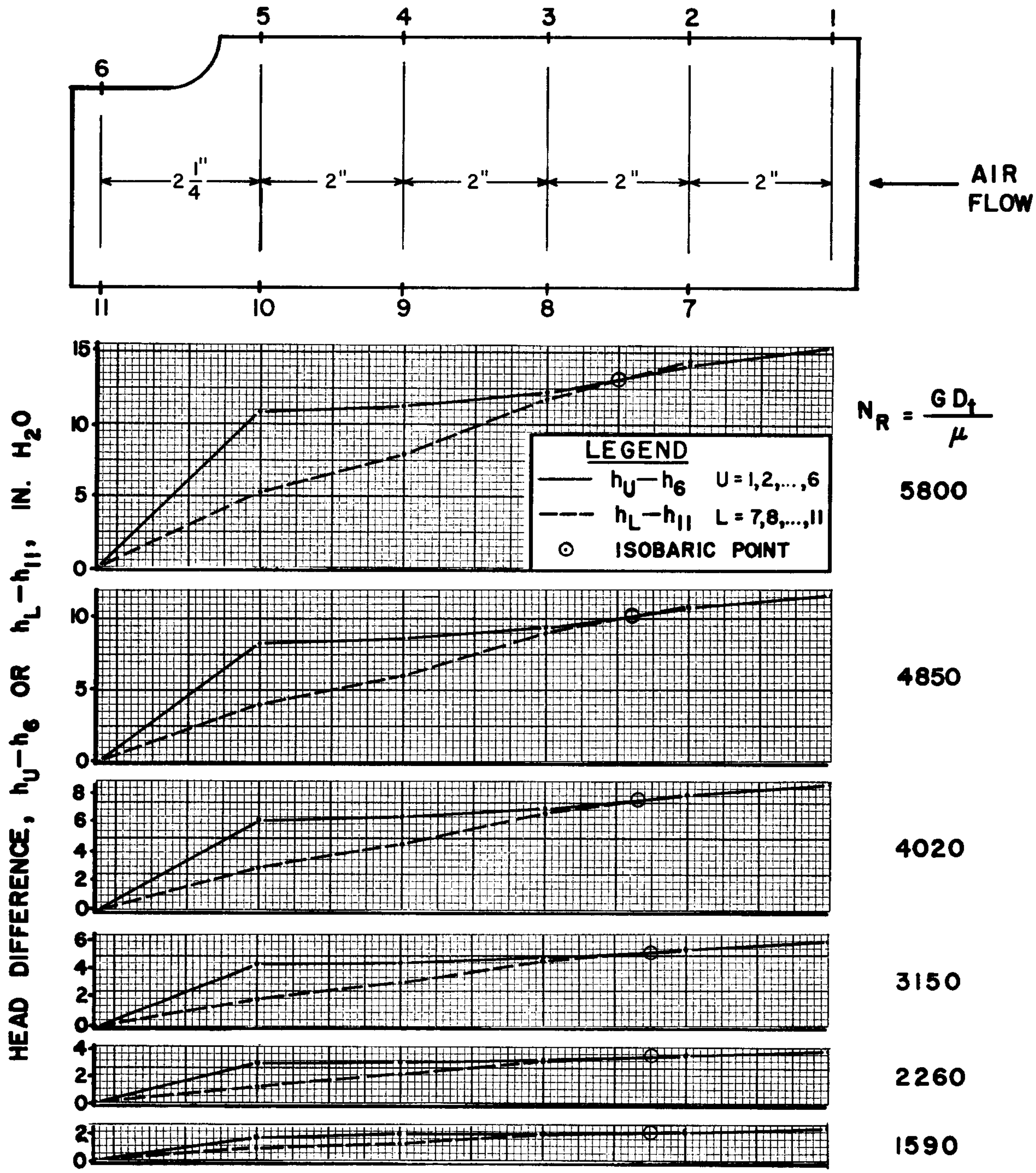

FIGURE NO. 6.1 - FIRST HEAT EXCHANGER AIRFLOW MODEL. PRESSURE DISTRIBUTIONS FOR VARIOUS FLOWS IN CROSS-FLOW REGION.

For the cross-flow tests, where air was the fluid used, it was found convenient to rewrite equations (3) and (4) directly in terms of the measured quantities:

$$f_c = .098 \frac{h' + h'_b}{h'_o + h'_b} \frac{\Delta h}{\Delta h_o} \tag{5}$$

and

$$N_R = 490 \sqrt{\Delta h_o (h'_o + h'_b)} \tag{6}$$

Equations (5) and (6) are developed in Appendix C.

Equations (5) and (6) were derived on the assumption that the flow was incompressible and isothermal, the change in air density between the air measuring orifice and the test section, however being taken into account. This assumption considerably simplified data processing; that it should lead to little error seemed reasonable, considering that the pressure drops were not in excess of 2 to 4 percent of the inlet pressures.

Figure 6.2 presents the results of the cross-flow tests on the first heat exchanger airflow model. Also plotted is the curve from reference 2 pertinent to the configuration used in the tests. It will be noted that the agreement at low Reynolds' numbers is poor, becoming fairly good for Reynolds' numbers of 5,000 to 10,000. The experimental results cross the reference curve at about 10,000, hooking down rather sharply thereafter. Unfortunately, sufficient data is not available to be able to say whether the hook is real or illusory.

That the cross-flow tests yield a curve different in form from the reference curve is not greatly surprising, considering the geometry differences for the two cases. The data on which the reference curve is based were for tube banks with all tubes perpendicular to the flow direction; the results reported here are for a region where there is a gradual transition from all tubes perpendicular to the flow direction to all tubes parallel to the flow. Furthermore, the perpendicular tubes are fairly widely spaced, whereas the parallel tubes are closely spaced; this would, undoubtedly, result in the open portions receiving a disproportionate share of the total flow.

It may be concluded that the precision of measurement in the cross-flow tests was good, as indicated by the small scatter in the experimental points; it is possible to draw a well-defined curve through the points. No such conclusion with respect to the reproducibility of the experimental curve should be drawn, however; a relatively small change in flow pattern could produce a marked change in the apparent friction factor.

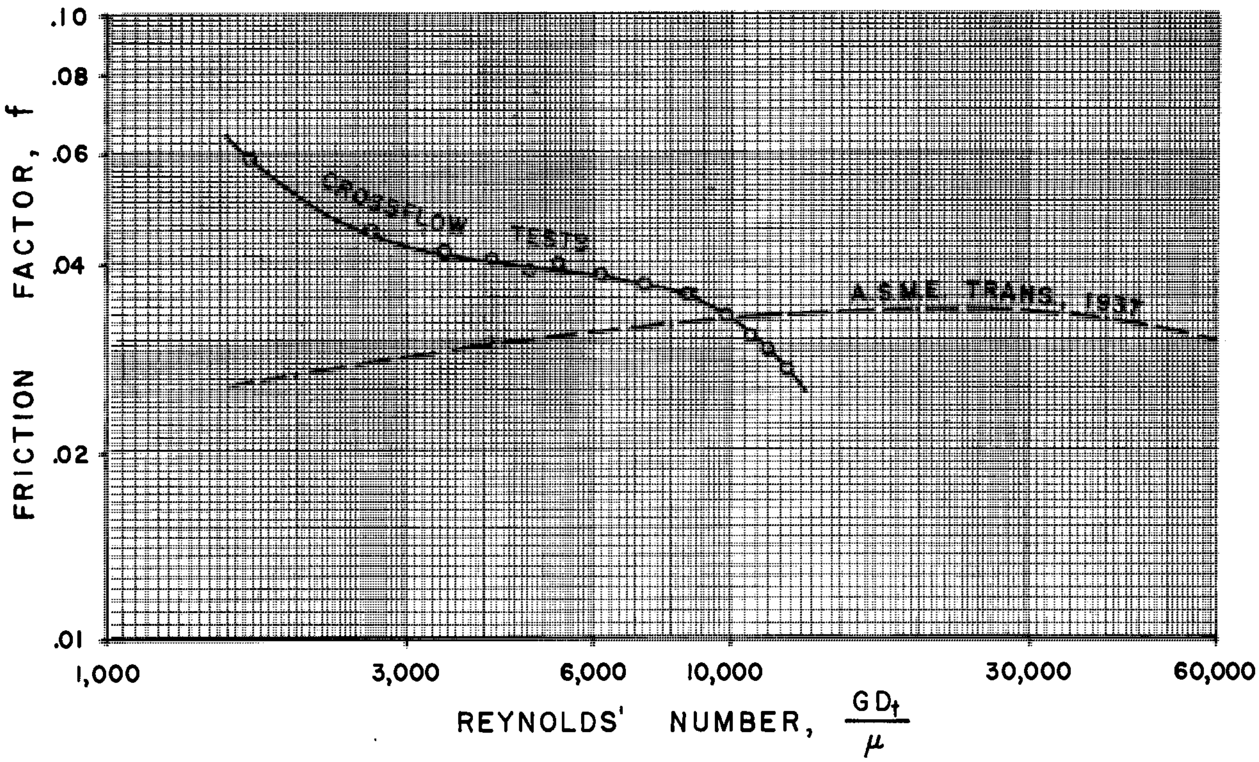

FIGURE NO. 6.2 - FIRST HEAT EXCHANGER AIRFLOW MODEL. CROSS-FLOW FRICTION FACTOR AGAINST REYNOLDS' NUMBER.

Because changes in proportions in the cross-flow region might be expected to lead to unavoidable and essentially unpredictable changes in the apparent friction factor, and because of the moderately good agreement with reference 2, it is felt that the friction factor data of reference 2 will yield a sufficiently good estimate of cross-flow losses. In a well-designed system the cross-flow losses will be a small fraction of the total losses, thus diminishing the need for a high degree of accuracy.

Parallel-Flow Tests

No pressure drop data for flow parallel to large numbers of closely spaced tubes could be found in the literature. However, because the components of such multiple flow passages are geometrically similar to certain noncircular ducts for which the equivalent diameter has been shown to be a satisfactory correlation parameter, it might be hypothesized that the equivalent diameter would be equally useful for parallel flow around tubes. Figure 7 summarizes the results of a series of tests on several geometries made to check this hypothesis. Geometries tested included:

1. Rectangular duct containing a 12 x 20 square pitch bundle of 1/8 inch diameter copper rods.

2. Smooth 1.1 inch inside diameter glass tube.

   (a) Empty.
   (b) Containing six hexagonally disposed brass tubes.

      1. 1/8 inch diameter.
      2. 3/16 inch diameter.
      3. 1/4 inch diameter.

3. Smooth 1.4 inch inside diameter stainless steel tube containing a 52 tube square pitch bundle of 1/8 inch outside diameter stainless steel tubes.

The friction factor was defined by the Darcy equation

$$f_p = \frac{\Delta H}{\frac{L}{De} \quad \frac{V^2}{2g}} \tag{7}$$

and the Reynolds' number in the tube bundle by

$$N_R = \frac{V \; De \; w}{\mu} \tag{8}$$

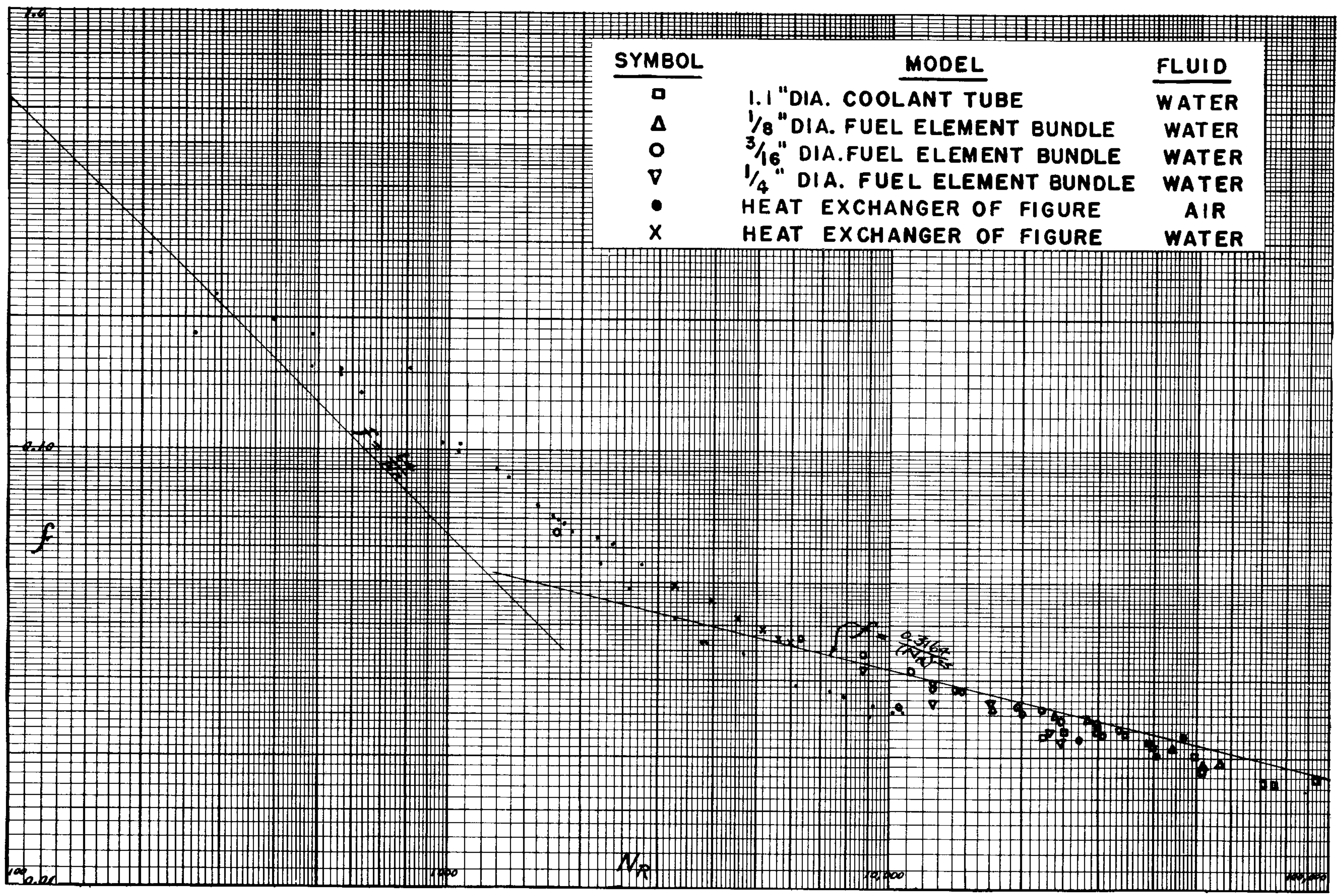

FIGURE 7. FRICTION FACTOR VS REYNOLD'S NUMBER FOR ALL MODELS TESTED.

For the airflow tests, equations (7) and (8) were written directly in terms of the measured quantities as

$$f_p = \left[\frac{De}{L}\right]\left[\frac{1}{C_d}\right]^2\left[\frac{A}{A_o}\right]^2 \frac{\Delta h}{\Delta h_o} \quad \frac{h' + h'_b}{h'_o + h'_b} \tag{9}$$

and

$$N_R = 21.08 \; \frac{A_o \, C_d \, De}{A \mu \sqrt{t_o + 460}} \; \sqrt{\Delta h_o \, (h'_o + h'_b)} \tag{10}$$

as shown in Appendix C.

For the water flow tests, equations (7) and (8), in terms of measured quantities, became

$$f_p = 656.9 \; \frac{DeA^2}{L} \; \frac{\Delta h'}{G^2} \tag{11}$$

and

$$N_R = 20.02 \; \frac{De}{A} \; G \tag{12}$$

as shown in Appendix D.

The agreement between the data and the predicted values is seen to be good except in the transition region. It has been shown (see, for example, reference 3, p. 22) that the equivalent diameter of noncircular sections does not give the friction factor as a unique function of Reynolds' number in laminar flow. For this reason, correlation in the transition region, where the nature of the flow is uncertain, cannot be expected to be as good as in the region of definitely turbulent flow. Note, however, that the data form a relatively smooth curve from the laminar to turbulent flow regions.

For Reynolds' numbers in excess of around 5,000, the mean of the data lies about 7% below the expected curve. However, the data for the non-circular flow passages are in good agreement with a base run on a smooth glass pipe of circular cross-section.

It is concluded that the equivalent diameter is a satisfactory correlation parameter for the region of definitely established turbulent flow in passages of the type encountered in fluid flow parallel to banks of tubes.

Heat Exchanger Spacer Tests

1. Spacer dimension correlation

The spacers used for the first and second heat exchanger models and for the liquid-to-liquid heat exchanger model were made from round wire rolled to the desired thickness. Figure 8 represents an attempt to correlate dimensions of the spacers with the diameters of the wires from which they were rolled. Data are presented for the copper spacers used in the first and second airflow models and for several samples of inconel spacers made for another heat exchanger (not reported here).

A plot of $d_w/t - 1$ against $w/t - 1$ necessarily passes through (0,0); hence, if a log-log plot of $d_w/t - 1$ against $w/t - 1$ results in a straight line, $d_w/t - 1$ may be expressed as a constant times some power of $w/t - 1$. It can be seen that the data of Figure 8 fit a single straight line quite well. The measured slope of the line is 0.96 and for $w/t = 2.00$, $d_w/t = 1.59$. Wire diameter, spacer thickness, and spacer width are therefore correlated by the equation

$$d_w/t = 1 + 0.59\ (w/t - 1)^{0.96} \qquad (13)$$

Note that, for the limited range of spacer materials used, the correlation is independent of the material.

2. Spacer friction factor correlation

The spacer friction factor is defined in this report as

$$f_s = \Delta H_s/(V^2/2g) \qquad (14)$$

where the velocity used is that in the tube bundle ahead of the spacers. In terms of the measured quantities, equation (14) becomes, from Appendix C,

$$f_s = \left[\frac{1}{C_d}\right]^2 \left[\frac{A}{A_o}\right]^2 \frac{\Delta h}{\Delta h_o} \quad \frac{h' + h'_b}{h'_o + h'_b} \qquad (15)$$

The Reynolds' number used was that in the tube bundle and is given by equations (8) and (10).

The spacer friction factor is shown in Figures 9.1 and 9.2 as a function of Reynolds' number in the tube bundle. Each curve is seen to

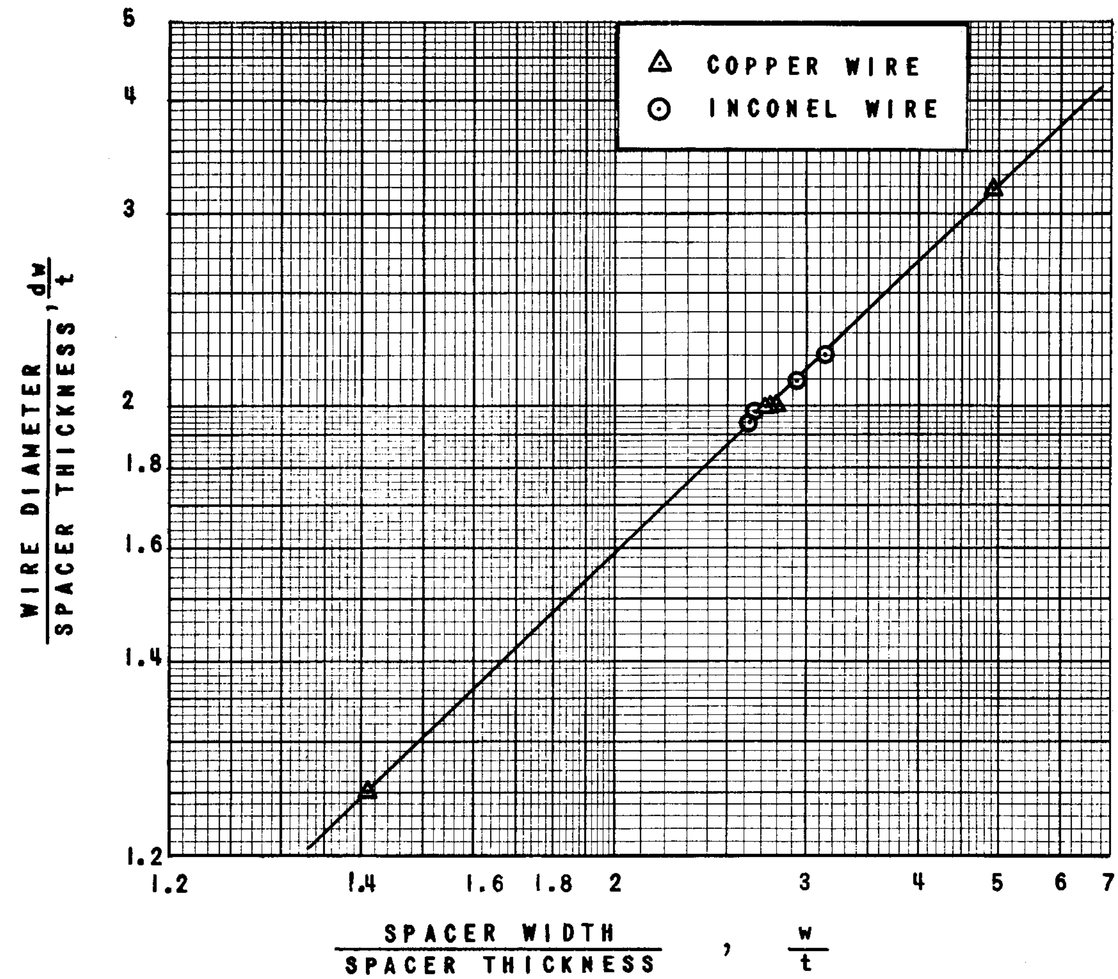

FIGURE NO. 8. - WIRE-DIAMETER-TO-SPACER-THICKNESS RATIO AGAINST SPACER WIDTH-TO-THICKNESS RATIO.

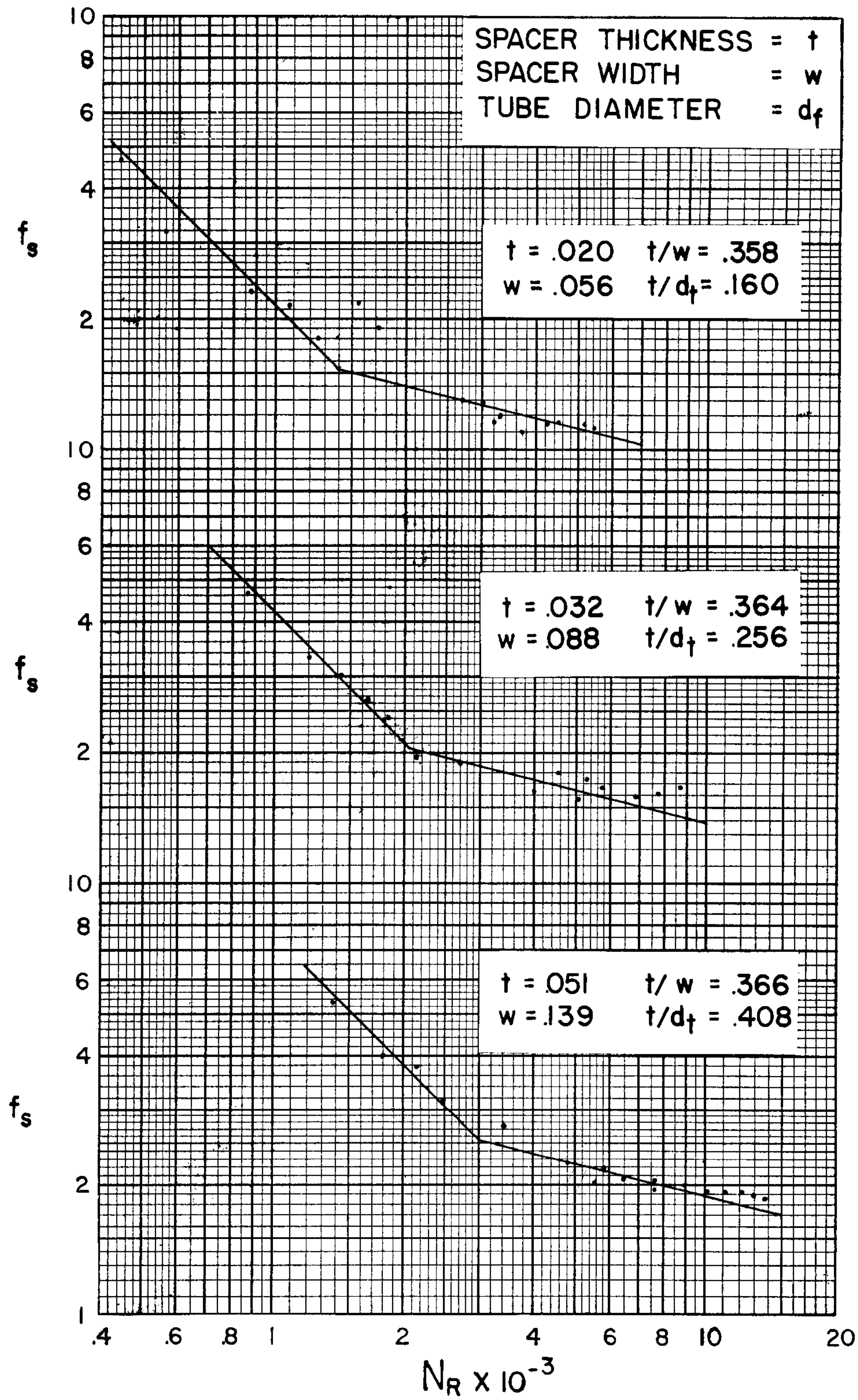

FIGURE NO. 9.1 SPACER FRICTION FACTOR AGAINST REYNOLDS' NUMBER IN TUBE BUNDLE. EFFECT OF SPACER-THICKNESS-TO-TUBE-DIAMETER RATIO AT CONSTANT SPACER THICKNESS-TO-WIDTH RATIO.

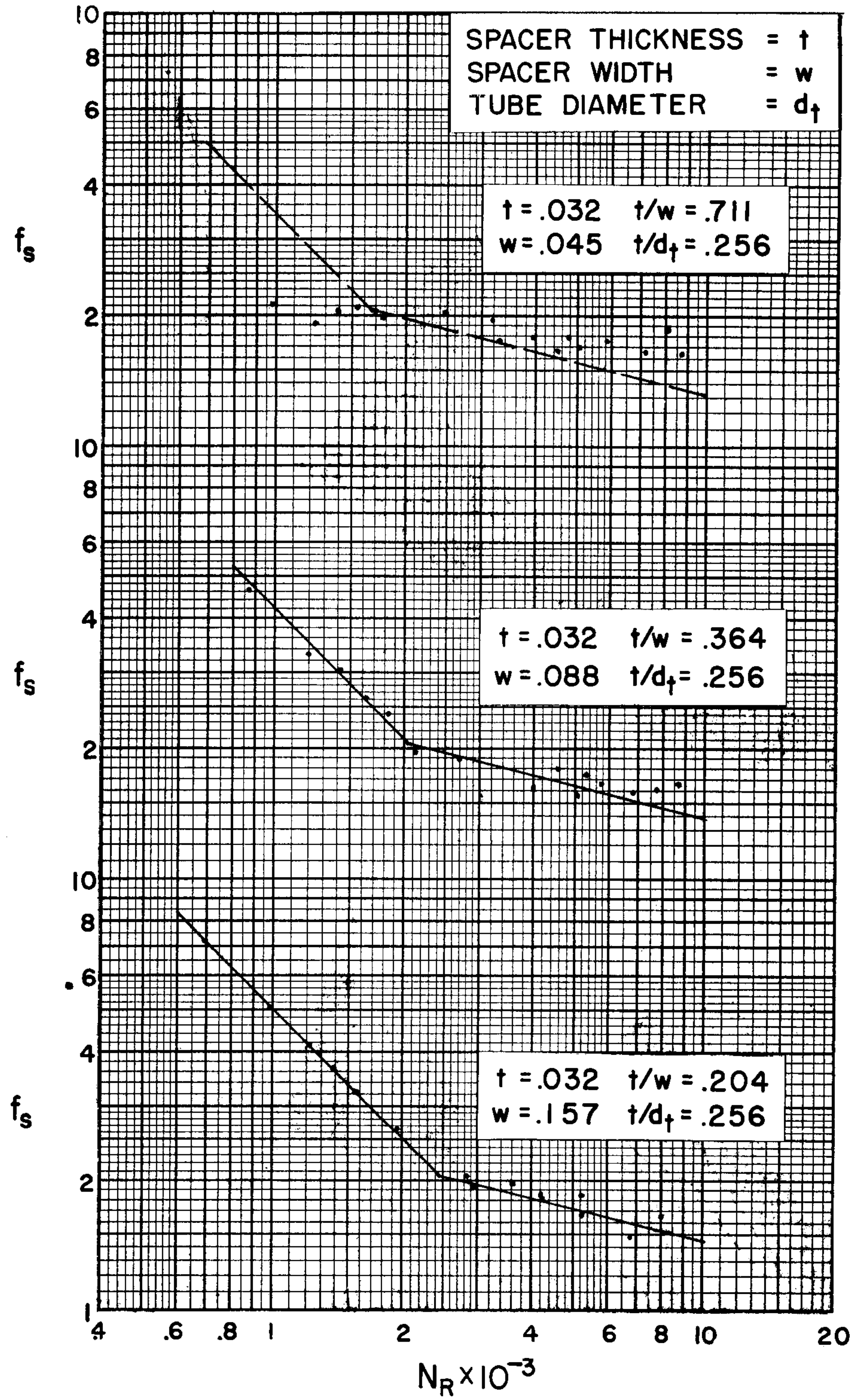

FIGURE NO. 9.2 SPACER FRICTION FACTOR AGAINST REYNOLDS' NUMBER IN TUBE BUNDLE. EFFECT OF SPACER THICKNESS-TO-WIDTH RATIO AT CONSTANT SPACER-THICKNESS-TO-TUBE-DIAMETER RATIO.

consist of two distinct branches, the left-hand branch having a slope of -1 (corresponding to the Hagen-Poiseuille slope for laminar flow) and the right-hand branch having a slope of -1/4 (corresponding to the Blasius slope for turbulent flow).

Figure 9.1 is a plot at constant spacer thickness-to-width ratio for three different spacer-thickness-to-tube-diameter ratios. It will be observed that the spacer thickness has a dual effect; both the critical Reynolds' number and the friction factor at that Reynolds' number increase with spacer thickness. That this is physically reasonable may be seen from the following considerations. It is easily shown that the ratio of the Reynolds' number in the tube bundle to that through the spacers increases with spacer thickness. Further, transition of the flow through the spacers from laminar to turbulent flow may reasonably be expected to occur at an approximately constant value of the spacer Reynolds' number. From this it follows that the tube bundle critical Reynolds' number should increase with spacer thickness, as it is, indeed, observed to do. The increase of f_s is undoubtedly ascribable simply to the increased obstruction to flow through the spacers as the thickness increases.

Figure 9.2 is a plot at constant spacer-thickness-to-tube-diameter ratio for three different spacer thickness-to-width ratios. Confining attention for the moment to the two lower curves, note that the effect of varying spacer proportions at constant thickness is to increase the critical Reynolds' number while leaving the friction factor at that number unchanged.

The anomalous behavior of the data in the top curve is unexplained; whether the deviation is an essential flow phenomenon or simply fortuitous is not known at present. A possible explanation is that the criterion used for spacer geometric similarity, i.e., the thickness-to-width ratio, is invalid when the spacer differs little from a cylinder, as in the present case.

Because of the failure of this set of data to conform to the general pattern, only the data for the four remaining sets of spacers were used for correlation. Then, from the generalized curve so obtained, the curve shown as a dashed line in the upper portion of Figure 9.2 was superimposed on the deviant data. It will be noticed that except for two or three points at each end of the data range the curve fits the data moderately well.

As a first step in correlating the spacer data, a correction factor of the form $(t/w)^m(t/d_t)^n$ was applied to the tube bundle Reynolds' number in order to reduce the critical Reynolds' numbers for all the spacers to a common value. The exponent m was determined from the slope of the straight line logarithmic plot of critical Reynolds' number against t/w for constant t/d_t. The exponent n was found from a similar plot for t/d_t at constant t/w.

The results of the initial correlation are shown in Figure 9.3. All five sets of data have now been adjusted to a critical modified Reynolds' number of approximately 4300. Note the close correlation between the data for t/w = .364 and that for t/w = .204. Again it will be observed that, except for two or three points at each end of the range, the data for t/w = .711 fit well with the other two sets of data.

Figure 9.3 shows clearly that the modification required on f_s involves only t/d_t. A correction factor of the form $(t/d_t)^p$ was therefore applied to f_s in order to reduce the data in Figure 9.3 to a single curve. The exponent p was determined from the slope of the straight line logarithmic plot of friction factor against t/d_t at a constant value of modified Reynolds' number.

The final data correlation is shown in Figure 9.4. In general, the correlation appears quite good, the data scattering quite evenly (with several notable exceptions) about the mean curve. It is felt that the observed scatter may be attributed at least in part to the random fluctuations with which the compressed air supply to the model was cursed.

It may be noted that the right-hand end of the correlation curve seems low relative to the data points. However, this apparent effect is due primarily to the anomalous data previously discussed. Deletion of the last few points for the t/w = .711 data gives a good fit.

Liquid-to-Liquid Heat Exchanger Tests

1. Flow around tubes

Components of losses for isothermal flow around the heat exchanger tubes are shown in Figure 10.1 as a function of Reynolds' number in the tube bundle. The over-all losses were obtained from water flow tests on the complete exchanger. Inlet and outlet losses are estimated values obtained from the equations for head losses in sudden expansions and contractions (see, for example, reference 4). Spacer losses were determined from the data in Figure 9.1, this exchanger having spacers .020 in. thick.

The effective length of the tube matrix was determined in two independent ways (which checked each other gratifyingly). From Figure 3.1, the effective length was estimated, by eye, to be 11 inches. Deduction of inlet and outlet losses and spacer losses from the over-all curve gave a residual curve of losses chargeable to the matrix. Comparison of this curve with that obtained for a 3-inch section of the matrix gave an effective length of 11 inches, the value used in Figure 10.1.

At a Reynolds' number of 3,000 the inlet and outlet, spacer, and matrix losses contribute roughly equally to the over-all losses. This

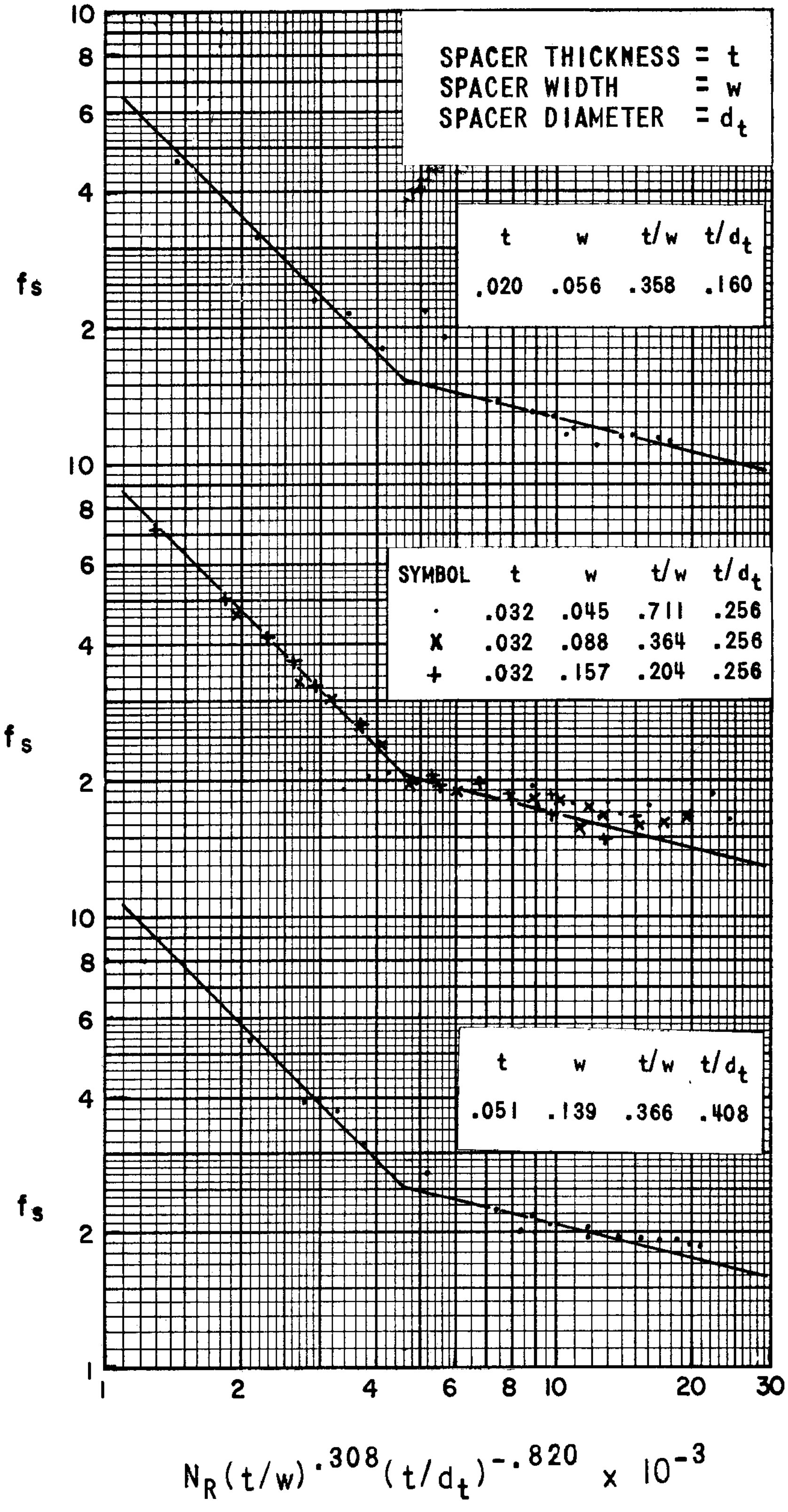

FIGURE NO. 9.3 - SPACER FRICTION FACTOR AGAINST MODIFIED REYNOLDS' NUMBER. INITIAL DATA CORRELATION.

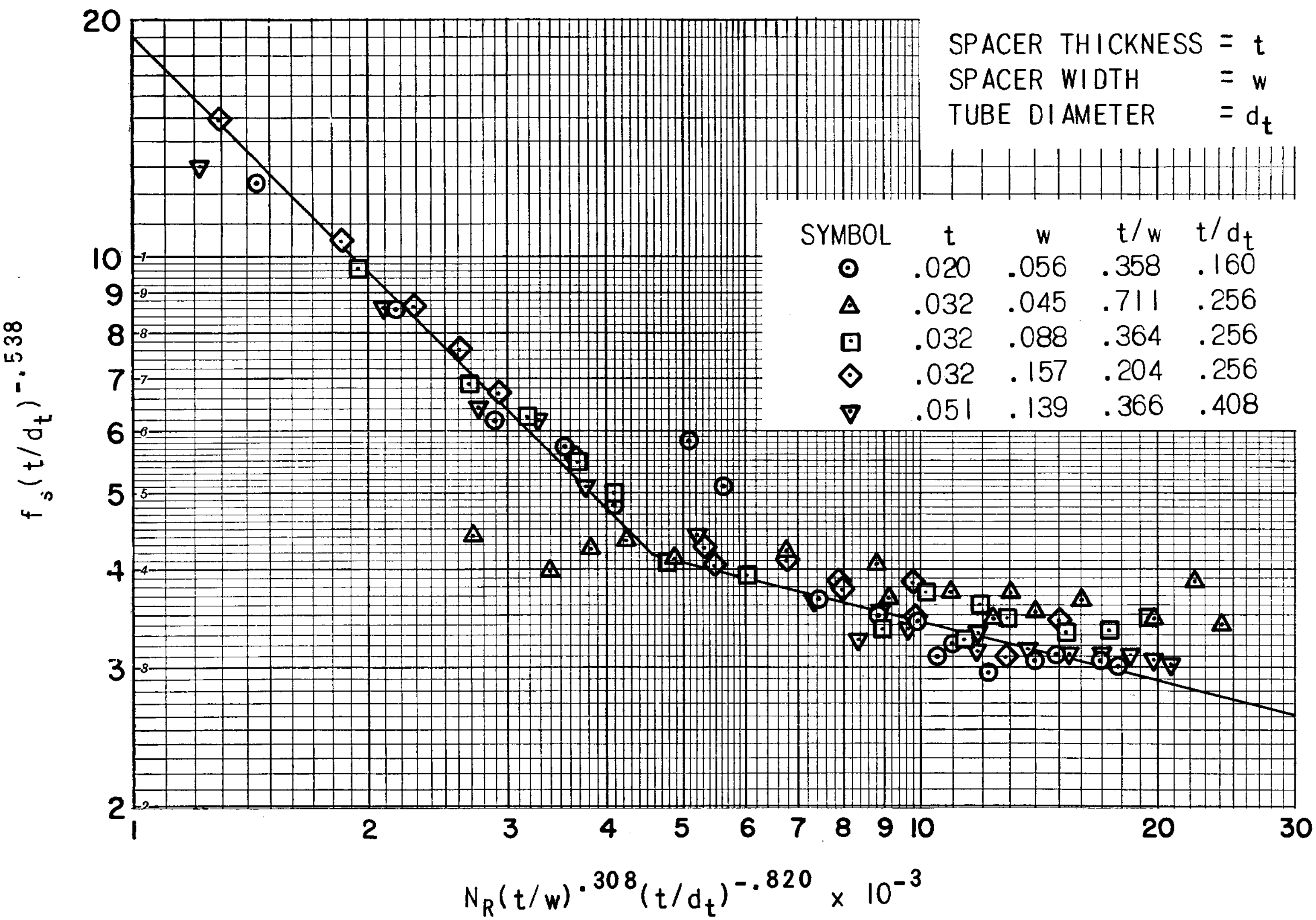

FIGURE NO. 9.4 - MODIFIED SPACER FRICTION FACTOR AGAINST MODIFIED REYNOLDS' NUMBER. FINAL DATA CORRELATION.

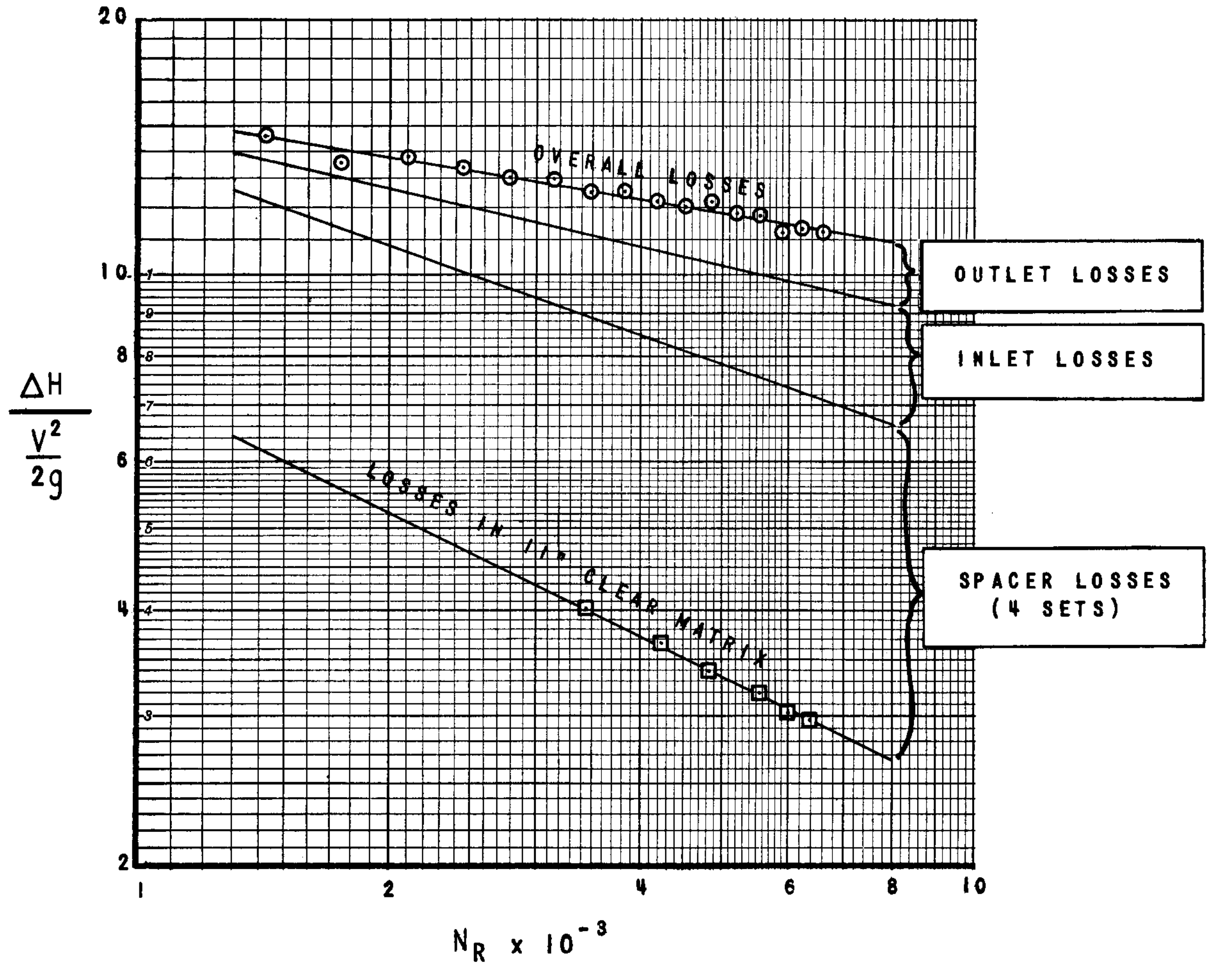

FIGURE NO. 10.1 - LIQUID-TO-LIQUID HEAT EXCHANGER MODEL. COMPONENTS OF LOSSES FOR ISOTHERMAL FLOW AROUND TUBES AGAINST REYNOLDS' NUMBER IN TUBE BUNDLE.

high proportion of losses chargeable to elements other than the tube matrix can certainly be reduced by judicious refinement of design. For example, elimination of a large part of the expansions and contractions could reduce the inlet and outlet losses to one-half to one-third their present values. The exchanger is sufficiently short that more sets of spacers are used per foot than really necessary; reduction of losses here by wider spacing should approximate one-half. The net result is that over-all losses should be reducible to sixty percent to two-thirds those obtained here.

2. Flow through tubes

If it is assumed that (1) the head losses for all tubes are the same, and (2) the friction factor for flow in each tube follows the Blasius relation (see Figure 7), then the following relation can be shown to hold:

$$\left[G_i^{1.75} D_i^{-4.75} L_i\right] \Big/ \overline{\left[G^{1.75} D^{-4.75} L\right]} = 1 \qquad (16)$$

Equation (16) is developed in Appendix E.

In order to test this relation, flows from each of the 52 tubes of the heat exchanger matrix were measured. The inside diameters of all the tubes were then checked, using a set of number drills as plug gauges. Equivalent lengths of the tubes were determined from the print in Figure 3.1. An equivalent length was obtained for each row by taking the average physical length of the tubes in the row plus an allowance for two 90° bends.

The parameters so obtained were used in equation (16) to arrive at the plot in Figure 10.2. The figure shows that the assumed relation correlates flow, tube diameter, and equivalent length fairly well. All points are within 20 percent of the mean, with only 3 points being 15 or more percent from the mean.

At least part of the observed scatter could be attributed to the following causes. For each row a single equivalent length was used for simplicity. Examination of Figure 3.1 will show that this is not quite correct. Both the physical lengths and bend allowances vary somewhat. Further, even where the specified lengths and bend radii are the same, the possibility of irregularities exists, e.g., slight kinks, etc. In addition, the cone-arc welding at one end of the heat exchanger produced some necking down of the inside diameter. This was not taken into account.

Fuel Element Spacer Tests

Figure 11.1 presents a comparison of over-all velocity head losses for a 3/16 inch tube fuel element fitted with several different tube spacers.

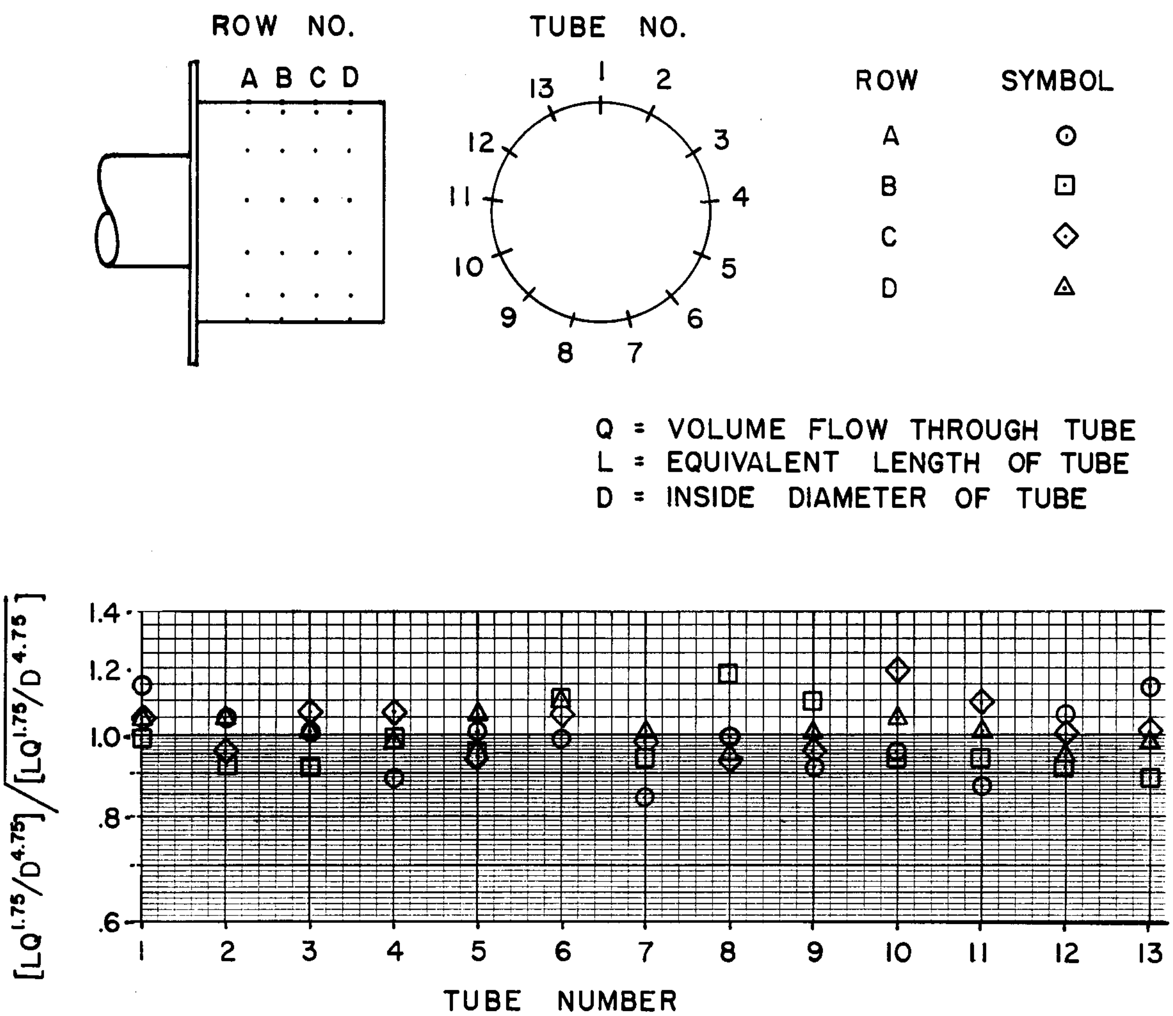

FIGURE NO. 10.2 - LIQUID-TO-LIQUID HEAT EXCHANGER MODEL.
CORRELATION OF FLOWS THROUGH INDIVIDUAL
TUBES WITH TUBE LENGTH AND DIAMETER.

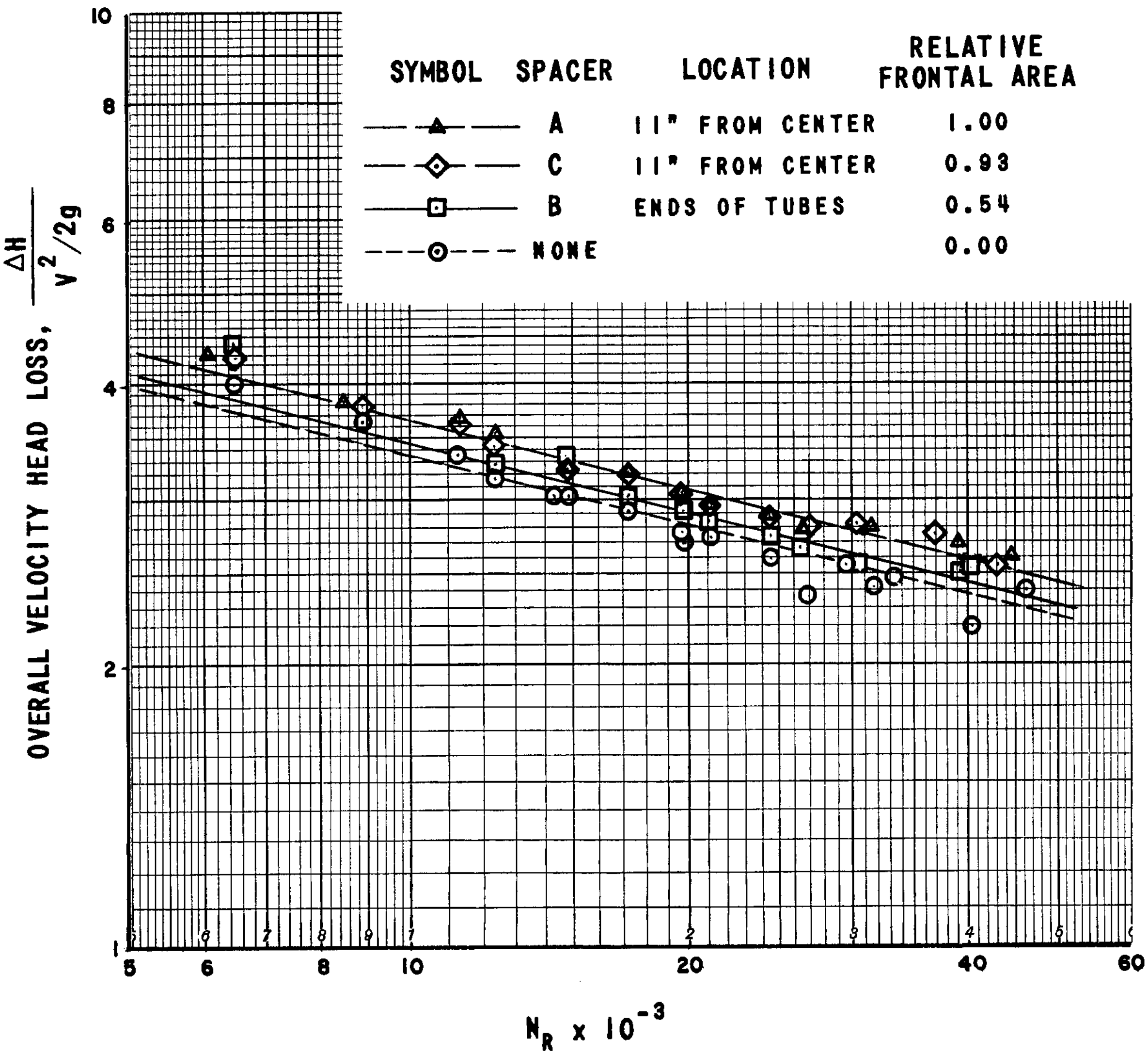

FIGURE NO. 11.1 - FUEL ELEMENT MODELS. VELOCITY HEAD LOSSES FOR VARIOUS FUEL TUBE AND SPACER CONFIGURATIONS AGAINST REYNOLDS' NUMBER IN TUBE BUNDLE.

The fuel element is shown in Figure 4.1; the spacers are illustrated in Figure 4.3. The lower dashed line in Figure 11.1 represents a base run made with the fuel element and no added spacers. The solid line shows the effect of placing 2 of the B spacers on the fuel element, one at each end. The upper dashed line represents the results for both the A and C spacers. Two spacers of each type were used, being placed about midway between the center and ends of the fuel element.

Because of the evident difficulty in attempting to disentangle the data in a plot such as Figure 11.1 sufficiently to draw distinct curves, the four sets of data were first plotted on separate sheets; the separate curves were then drawn and transferred to the composite plot.

It can be seen that spacers A and C, similarly placed and having nearly the same frontal area, show no difference in losses. Spacer B, however, with a frontal area slightly over half that of spacer A, shows a considerably reduced incremental head loss (about 3 percent, compared with about 8 percent for A and C). Spacers B were, however, placed near the tube ends in order to keep them in position without soldering. The effect of position on losses was, therefore, checked with one of the other spacers.

The effect of spacer position on over-all losses is shown in Figure 11.2 for spacer A. The base curve (no spacers) is included for comparison. The incremental loss is now seen to be about 12 percent for the end position, compared to 8 percent for the centrally placed spacer. There is, then, a fifty percent increase in the incremental loss when the spacer is in the end position. Applying this result to spacer B, the incremental loss for a central position would be reduced to about 2 percent. Note, however, that while the effect of spacer position on incremental loss is large, the effect on over-all loss is small, amounting to only 3 percent even for spacer A.

The net result is that the incremental loss chargeable to the spacers runs from about one to four percent (per spacer) of the velocity head in the tube bundle. The conclusion to be drawn is that the choice among several spacer designs (particularly if the frontal areas are roughly the same) should be based principally on ease of fabrication and installation.

It is of interest to compare the measured incremental loss for a spacer with losses calculated from elementary hydraulic theory. Such a comparison is made in Figure 11.3 for spacer A. The upper horizontal line represents the difference in velocity heads before and in the spacer; the lower horizontal line represents the loss expected from a sudden contraction and expansion. Notice that the spacer loss is intermediate between these values, approaching the contraction and expansion loss for high Reynolds' numbers. It is interesting to note that at a Reynolds' number of 10,000 the spacer loss is almost exactly the geometric mean of the calculated losses.

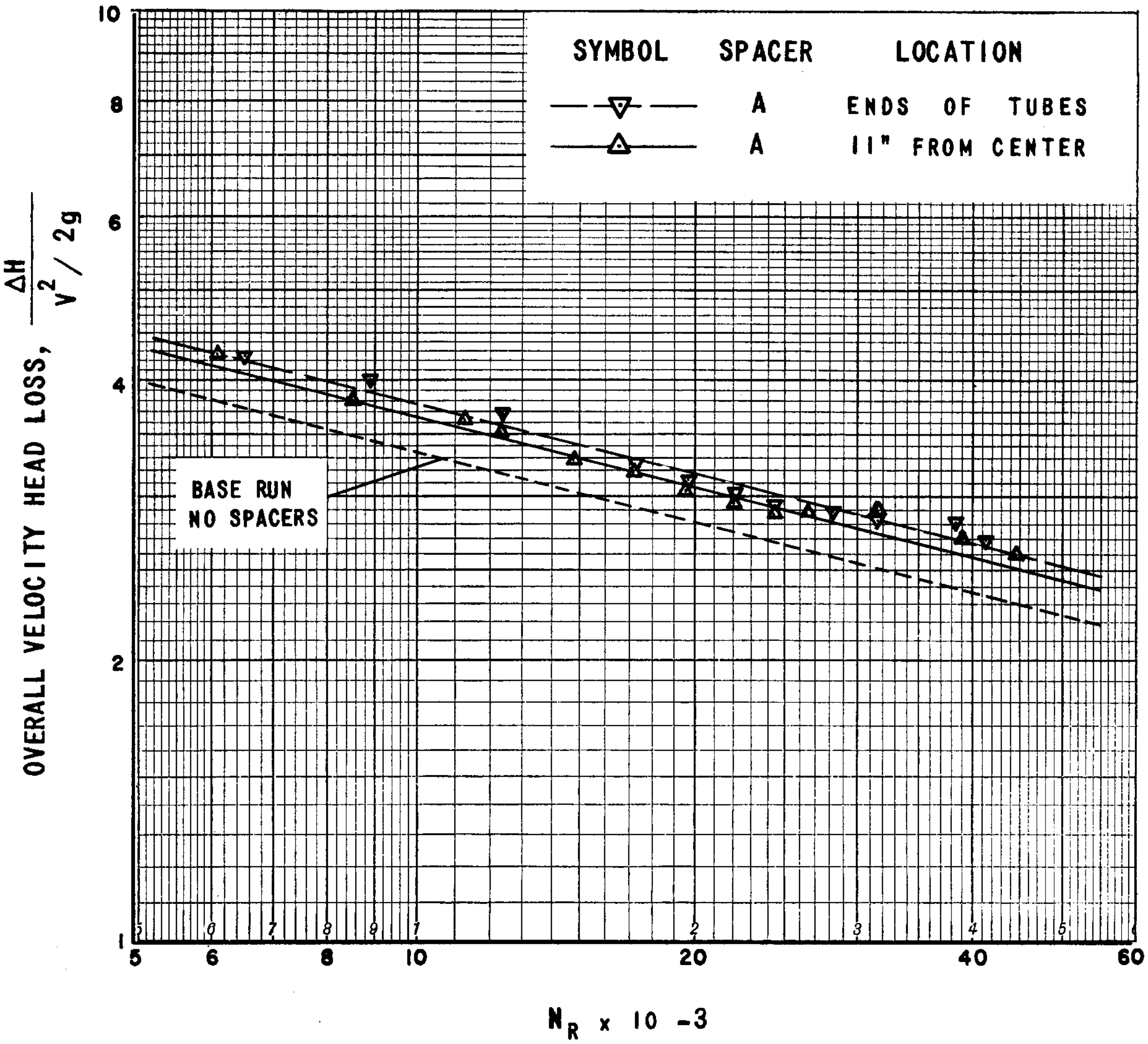

FIGURE NO. 11.2 - FUEL ELEMENT MODELS. EFFECT OF SPACER POSITION ON VELOCITY HEAD LOSSES FOR A FUEL TUBE SPACER.

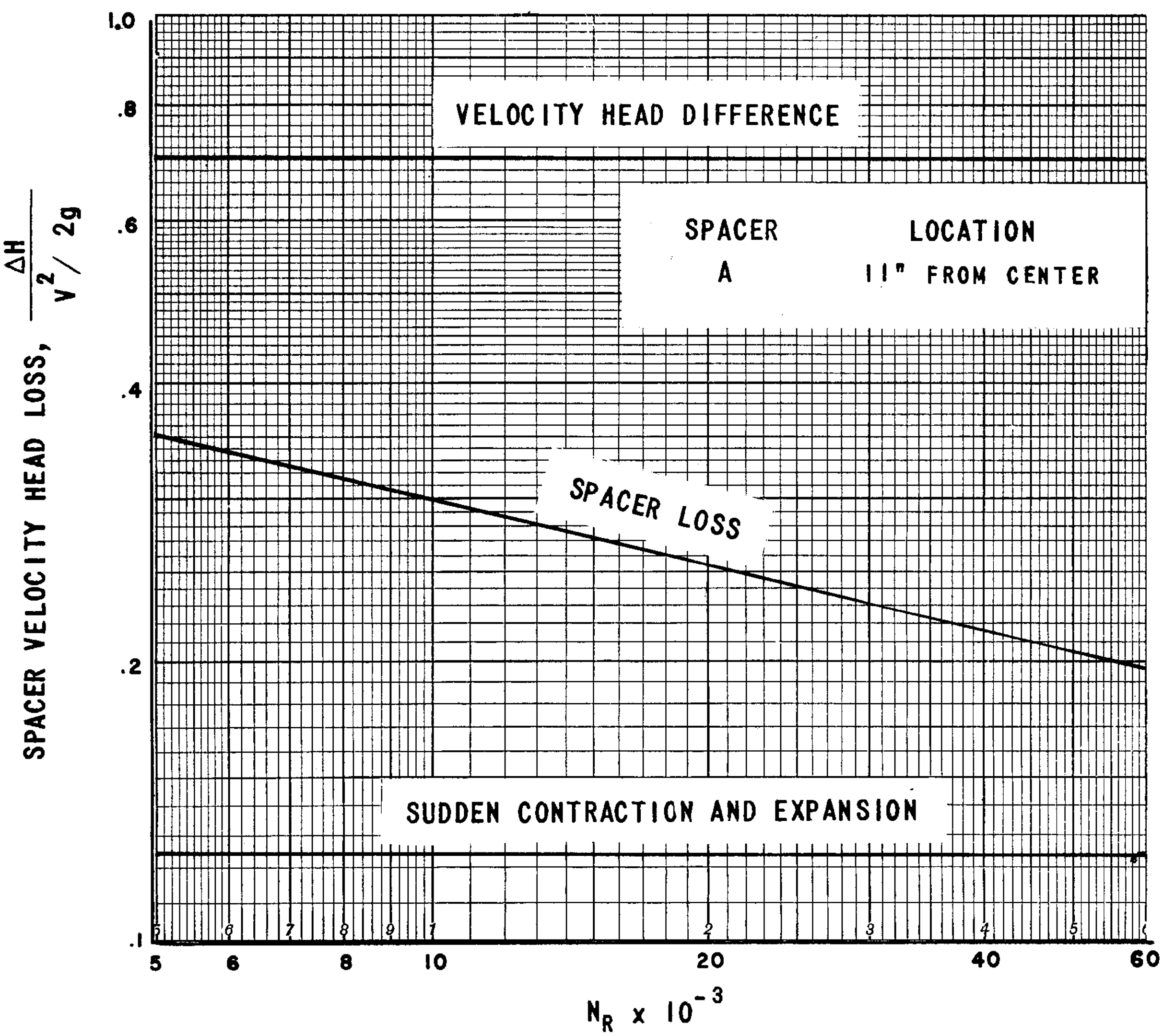

FIGURE NO. 11.3 - FUEL ELEMENT MODELS. MEASURED AND CALCULATED VELOCITY HEAD LOSSES FOR A FUEL TUBE SPACER AGAINST REYNOLDS' NUMBER IN TUBE BUNDLE.

That these results are at least reasonable can be seen from the following considerations. Spacer losses could be expected to be less than a velocity head difference inasmuch as there is sure to be some pressure recovery in the stream leaving the spacer, a fact that the velocity head difference fails to take into account. On the other hand, spacer losses might be expected to be larger than those from a sudden flow area change because of inevitable interference and frictional losses. These would be expected to diminish with increased Reynolds' number, resulting in the tendency for the spacer and area change loss curves to converge.

HEAT EXCHANGER TEST LOOP

The results of a metallographic examination of the liquid-to-liquid heat exchanger of Figure 3.1 have recently been made available in the form of an ORNL memorandum by E. E. Hoffman of the ORNL Metallurgy Division and are appended to this report as Appendix F. The pertinence of this memorandum to the practicability of the proposed heat exchanger geometry and the fact that the information would not otherwise be published have dictated its inclusion. The following paragraphs are to supplement the information in the memorandum with some data on the heat exchanger test loop and its operation.

The liquid-to-liquid heat exchanger was operated for over 3,000 hours with NaK as the circulating fluid. Of this time, 175 hours were with inlet temperatures ranging from 800 to 1200°F and about 2830 were with an inlet temperature of 1500°F. Operating conditions during the endurance run are summarized in Table II.

Table II

Operating Conditions for Heat Exchanger Endurance Run

NaK flow, gpm	5.2
Flow velocities, ft/sec	
Through tubes	5.2
Around tubes	1.9
Rest of loop	2.8
Temperatures, °F	
Inlet through tubes	1440
Outlet through tubes	870
Inlet around tubes	1500
Outlet around tubes	930

Previous loops have circulated the entire flow through the header; this practice resulted in a thorough churning of the fluid in the header tank, rendering it completely ineffective in its intended role as a settling tank and neatly returning oxide and other debris to the circulating system. In an attempt to obviate this defect the header tank for this heat exchanger test loop was placed in a by-pass circuit and an orifice was used to restrict the flow in this secondary circuit and header tank to roughly five percent of that in the main loop. A sintered stainless steel filter was installed in the by-pass loop downstream of the header tank in order to catch any debris that failed to settle out in the header.

Some indication of the efficacy of this arrangement may be gained from the fact that for over 2,000 hours of operation no trouble was encountered anywhere in the loop from oxide accumulations. After around 2,100 hours total operating time some difficulty was experienced with short-circuiting of the spark plug probes used as sensing elements in the system level control. This shorting necessitated several brief shutdowns in order to clean the probes. At about 2,200 hours a voluntary shutdown was made for a thorough cleaning of the header tank and filter. A brief examination of the header tank and filter disclosed the presence of a considerable incrustations of a grayish material. After cleaning and reassembling of the header and filter into the by-pass loop, the system was again started up and operated without further incident to the voluntary termination of the endurance run at over 3,000 hours.

Visual examination of the heat exchanger prior to its release to the metallurgists disclosed a number of cracks in the tubes at the nicrobrazed end. These fractures appeared to be typical fatigue failures. The cracked tubes also showed considerable etching of their surfaces.

The alternating current electromagnetic pump used in the heat exchanger test loop caused the whole piping system to vibrate during operation so that it gave off a loud 120 cycle hum. This pump was mounted in the same vertical run of pipe as the heat exchanger as shown in Figure 3.6, the inlet to the pump being approximately 6 inches above the exit from the heat exchanger. Sixty-cycle alternating current was applied to the pump, giving 120 pressure pulses per second in the system. Operating for 3,000 hours therefore resulted in the application of nearly 22,000,000 pulses to the NaK in the system and, thence, to the tubes in the heat exchanger.

Minute cracks in three welds at the cone-arced end had been detected during a pressure test made immediately after welding. No attempt was made to repair these cracks as it was felt they were unlikely to give trouble.

CONCLUSIONS

1. The proposed heat exchanger construction employing flow parallel to the tubes in the region around the tubes has been shown to be quite practical and to yield such low pressure drops that the design of heat exchangers much more compact than the conventional cross-flow tube-and-shell type is now practicable.

2. At low flows (4 to 5 gpm) measured values of the over-all heat transfer coefficient were about 40% below those computed from Lyon's equation. The agreement at higher flows (of the order of 20 gpm) was good.

3. Operation at 1500°F inlet temperature had negligible effect on heat transfer over a period of at least 2,000 hours.

4. Heat exchanger pressure drops showed no change with operating time, the observed scatter being random and of a size commensurate with careful gauge reading.

5. Cross-flow friction factors can be computed with sufficient accuracy from reference 2.

6. Losses in heat exchanger cross-flow regions can be kept quite small in comparison with the frictional losses in the tube bundle.

7. No tube flutter excited by fluid flow was observed for distances between sets of similarly placed spacers as high as 70 tube diameters.

8. Friction factors for flow around tubes correlate well with the Blasius equation on an equivalent diameter basis.

9. Spacer friction factors correlate well with spacer and model parameters.

10. For turbulent flow in the heat exchanger tube bundle, losses chargeable to the spacers can be kept to about half the frictional losses for the tubes alone.

11. Heat exchanger inlet and outlet losses can be estimated with sufficient accuracy from conventional hydraulic theory using the sudden expansion and contraction formulas.

12. Losses for flow both through and around tubes may be predicted with reasonable accuracy.

13. Head losses for the fuel tube spacers are conservatively estimated from the difference in velocity heads before and in the spacer.

14. Differences in losses for the various fuel tube spacer designs were small.

15. The effect of spacer position on spacer losses was negligible.

16. The choice among spacer designs that restrict the flow passage by essentially the same amount should be based primarily on ease of fabrication and installation.

REFERENCES

1. Lyon, R. N., "Forced Convection Heat Transfer Theory and Experiments with Liquid Metals," ORNL-361, 21, (1949)

2. Grimison, E. D., "Correlation and Utilization of New Data on Flow Resistance and Heat Transfer for Cross Flow of Gases Over Tube Banks," Trans. Am. Soc. Mech. Eng., 59, 583-594 (1937).

3. Kemler, E., " A Study of the Data on the Flow of Fluids in Pipes," Trans. Am. Soc. Mech. Eng., 55, HYD-55-2-7 (1933).

4. Vennard, J. K., Elementary Fluid Mechanics. Wiley and Sons, New York, 1940, pp. 169-175.

APPENDIX A

Symbols

The following symbols are used in this report:

A - Flow area, in^2.

C_d - Orifice discharge coefficient, dimensionless.

c_p - Specific heat, BTU/lb ^oF

d - Diameter, inches.

D - Diameter, feet.

f - Friction factor, dimensionless.

g - Acceleration of gravity, 32.2 ft/sec^2.

G - Volume flow, gpm.

h' - Head, in. Hg.

$\Delta h'$ - Differential head, in. Hg.

Δh - Differential head, in. water.

ΔH - Differential head, feet of fluid.

L - Length in direction of flow, feet.

N - Number of tubes in direction of flow.

t - Temperature, ^oF, or spacer thickness, inches (as indicated by context).

UA - Over-all heat transfer coefficient, BTU/hr ^oF.

V - Flow velocity, ft/sec.

w - Specific weight, lb/ft^3, or spacer width, inches (as indicated by context).

W - Weight flow, lb/sec.

η - Cooling effectiveness, degrees temperature change per degree inlet-temperature difference.

APPENDIX A (Continued)

μ - Absolute viscosity, lb/ft sec.

Subscripts:

- b - Barometer
- c - Cross-flow
- e - Equivalent
- o - Orifice
- p - Parallel-flow
- s - Spacer
- t - Tube
- w - Wire

- 1 - Heat exchanger inlet for flow around tubes.
- 2 - Heat exchanger outlet for flow around tubes.
- 3 - Heat exchanger inlet for flow through tubes.
- 4 - Heat exchanger outlet for flow through tubes.

APPENDIX B

COOLING EFFECTIVENESS AND OVER-ALL HEAT TRANSFER COEFFICIENT

Cooling effectiveness is defined by

$$\eta = \frac{t_1 - t_2}{t_1 - t_3}$$

Because $\quad t_1 - t_2 = t_4 - t_3$

it follows that

$$t_1 - t_2 = (t_1 - t_2 - t_3 + t_4)/2 \qquad \text{(B1)}$$

and, therefore,

$$\eta = \left(1 + \frac{t_4 - t_2}{t_1 - t_3}\right)/2 \qquad \text{(1)}$$

which is equation (1) of the text.

The over-all heat transfer coefficient is defined by

$$UA = Wc_p \frac{t_1 - t_2}{t_1 - t_4} \qquad \text{(B2)}$$

Because $\quad t_1 - t_4 = t_2 - t_3$

it follows that

$$t_1 - t_4 = (t_1 + t_2 - t_3 - t_4)/2 \qquad \text{(B3)}$$

Then, from equations (B1), (B2), and (B3),

$$UA = Wc_p \frac{t_1 - t_2 - t_3 + t_4}{t_1 + t_2 - t_3 - t_4}$$

which reduces to

$$UA = Wc_p \frac{\eta}{1 - \eta} \qquad \text{(B4)}$$

In terms of gallons per minute equation (B4) becomes

$$UA = 105.6\ G \frac{\eta}{1 - \eta} \qquad \text{(2)}$$

which is equation (2) of the text.

APPENDIX C

FRICTION FACTOR AND REYNOLDS' NUMBER FOR AIRFLOW TESTS

Friction Factor:

Define a friction factor, f by

$$f = \frac{\Delta H}{\frac{V^2}{2g}} \tag{C1}$$

The continuity equation,

$$A = \frac{w_o A_o V_o}{wA} \tag{C2}$$

the orifice equation for incompressible flow,

$$V_o = C_d \sqrt{2g\ \Delta H_o} \tag{C3}$$

and the equation of state for isothermal flow,

$$\frac{w_o}{w} = \frac{h'_o + h'_b}{h' + h'_b} \tag{C4}$$

when combined with equation (C1) yield

$$f = \left[\frac{1}{C_d}\right]^2 \left[\frac{A}{A_o}\right]^2 \frac{\Delta H}{\Delta H_o} \left[\frac{h' + h'_b}{h'_o + h'_b}\right]^2 \tag{C5}$$

But $$\frac{\Delta H}{\Delta H_o} = \frac{\Delta h}{\Delta h_o} \frac{w_o}{w}$$

$$= \frac{\Delta h}{\Delta h_o} \frac{h'_o + h'_b}{h' + h'_b} \tag{C6}$$

Finally, from equations (C5) and (C6)

$$f = \left[\frac{1}{C_d}\right]^2 \left[\frac{A}{A_o}\right]^2 \frac{\Delta h}{\Delta h_o} \frac{h' + h'_b}{h'_o + h'_b} \tag{C7}$$

The cross-flow friction factor is defined as

$$f_c = \frac{\Delta H}{4N \dfrac{V^2}{2g}}$$

Hence,

$$f_c = \frac{1}{4N} f \tag{C8}$$

which yields equation (5) of the text.

The parallel-flow friction factor is defined as

$$f_p = \frac{\Delta H}{\dfrac{L}{D_e} \dfrac{V^2}{2g}}$$

Hence,

$$f_p = \frac{D_e}{L} f \tag{C9}$$

which yields equation (9) of the text.

The spacer friction factor is defined as

$$f_s = \frac{\Delta H}{\dfrac{V^2}{2g}}$$

Hence,

$$f_s = f \tag{C10}$$

which yields equation (15) of the text.

Reynolds' Number:

Reynolds' number is defined by

$$N_R = \frac{DVw}{\mu} \tag{C11}$$

From equation (C2), (C3), and (C11)

$$N_R = \frac{DC_d A_o w_o \sqrt{2g\Delta H_o}}{\mu A} \tag{C12}$$

But

$$\Delta H_o = \frac{62.4}{12} \frac{\Delta h_o}{w_o} \tag{C13}$$

and

$$w_o = .0765 \frac{h'_o + h'_b}{29.92} \frac{519}{t_o + 460} \tag{C14}$$

Combining equations (C12), (C13), and (C14), and simplifying, then gives

$$N_R = 21.08 \frac{A_o C_d D}{A\mu \sqrt{t_o + 460}} \sqrt{(h'_o + h'_b)\, \Delta h_o} \tag{C15}$$

For the cross-flow Reynolds' number, equation (C15) was used with $D = D_t$, giving equation (6) of the text.

For the parallel-flow and spacer Reynolds' numbers, equation (C15) was used with $D = D_e$, giving equation (10) of the text.

APPENDIX D

FRICTION FACTOR AND REYNOLDS' NUMBER FOR WATER FLOW TESTS

Friction Factor

The friction factor is defined by the Darcy equation

$$f_p = \frac{\Delta H}{\frac{L}{De}\,\frac{V^2}{2g}} \tag{D1}$$

A mercury manometer was used to measure the differential head; hence,

$$\Delta H = \frac{12.6}{12}\,\Delta h' = 1.05\,\Delta h' \tag{D2}$$

Flow was measured in gallons per minute with a rotameter; hence,

$$V = \frac{231}{720}\,\frac{G}{A} \tag{D3}$$

Then, from equations (D1), (D2), and (D3),

$$f_p = 656.9\,\frac{DeA^2}{L}\,\frac{\Delta h'}{G^2} \tag{11}$$

which is equation (11) of the text.

Reynolds' Number

Reynolds' number is given by

$$N_R = \frac{V\,De\,w}{\mu} \tag{D4}$$

The range of water temperatures was sufficiently small that changes in specific weight of the water were negligible; w was taken as 62.4 lb/ft^3. Then from equations (D3) and (D4),

$$N_R = 20.02\,\frac{De}{A\mu}\,G \tag{12}$$

which is equation (12) of the text.

APPENDIX E

CORRELATION OF FLOW THROUGH INDIVIDUAL TUBES WITH TUBE LENGTH AND DIAMETER

For the i^{th} tube,

$$\Delta H_i = f_i (L_i/D_i)(V_i^2/2g) \tag{E1}$$

But,

$$V_i = (\pi/4)\ K_1\ (G_i/A_i)$$

$$= K_1\ (G_i/D_i^2) \tag{E2}$$

where K_1 = a constant

Also,

$$f_i = K_2\ N_{R\ i}^{-1/4}$$

$$= K_2\ (\mu/w)^{1/4} (V_i D_i)^{-1/4} \tag{E3}$$

where K_2 = a constant

Then, from equations (E1), (E2), and (E3),

$$\Delta H_i = K_1^{1.75} K_2\ (\mu/w)^{1/4} (1/2g)\ (G_i/D_i)^{-1/4} (L_i/D_i)(G_i^2/D_i^4)$$

$$= K\ G_i^{1.75} D_i^{-4.75} L_i \tag{E4}$$

In terms of average quantities,

$$\overline{\Delta H} = K\ \overline{\left[G^{1.75} D^{-4.75} L\right]} \tag{E5}$$

But the pressure drop across all tubes is the same; hence,

$$\overline{\Delta H} = \Delta H_i \quad \text{for all } i$$

and, therefore,

$$\left[G_i^{1.75} D_i^{-4.75} L_i\right] / \overline{\left[G^{1.75} D^{-4.75} L\right]} = 1 \tag{16}$$

which is equation (16) of the text.

APPENDIX F

METALLOGRAPHIC EXAMINATION OF HEAT EXCHANGER AFTER 3,000 HOURS OPERATION IN NaK

(By E. E. Hoffman, ORNL Metallurgy Division)

SUMMARY

From this investigation it is concluded that the tube failures detected in the Nicrobrazed tube-to-header were due to the vibration in the system and the etching effect which the circulating NaK had on the tubes in the hot zones. These failures were encouraged by the embrittlement of the areas near the joint by the brazing alloy and the large grain size of the 16 mil wall 304 stainless steel tubes. No fractures were detected in the 19.5 mil wall 347 stainless steel Nicrobrazed tube-to-header joints. One bad joint was found in the cone-arc welded header. This was probably due to faulty fabrication prior to welding, and had been noted as a slight leak in a pressure test made immediately after welding.

DISCUSSION

It was found on sectioning the heat exchanger that the hot end of the heat exchanger was very bright while the cold end was covered with a dark powdery film (Figures F1, F2). Spectrographic analysis of the dark and bright surface revealed the only detectable difference to be a Mn content present on the dark (cold zone) surface which was two to three times the expected value for 347 stainless steel. X-ray powder pattern of the dark powder scraped from the surface of a tube in the cold zone showed NiO, Cr and 347 stainless steel base material.

Of the 52 tubes in the heat exchanger, 37 were 1/8" O.D. with 19.5 mil wall and 15 were 1/8" O.D. with a 16 mil wall. These tubes were supposedly all 347 stainless steel, but it has been found by chemical analysis that the 16 mil tubes are actually 304 stainless steel. Approximately one-half of the thin wall 304 stainless steel tubes had visible cracks and the other half fractured when the tubes were bent slightly. The failures that occurred during the endurance test were approximately 1/16" to 1/32" from the header (Figures F3, F4). Figure F3 indicates the etching effect which the NaK produced on the surface of the tubes. It may also be seen in Figure F3 that the fracture was very brittle and seems to be along the grain boundaries. Figure F5 shows a Nicrobrazed tube-to-header joint which reveals the flowing characteristics of this alloy and the extremely large grain size of the thin 304 stainless steel tubing.

Figure F6 and F7 are photomicrographs of tube-to-header joints in the cold end of the heat exchanger which were cone-arc welded. Of eight such joints examined, Figure F7 is typical of seven of them, while one of the joints was faulty as illustrated by Figure F6. No attempt is made to explain the appearance of the joint in Figure F6, but it is doubtful that the tube was flush with the outside of the header prior to welding. All of the cone-arc welded joints had a tendency to shrink on cooling in the weld area causing a crevice between tube and header.

The tubes were cross sectioned at different points along the length of the heat exchanger and examined metallographically. The only apparent difference was in the grain size of the 19.5 mil wall 347 stainless steel tubing and the 16 mil 304 stainless steel tubing. Tubes shown in Figures F8, F9, F10, and F11 were cut from the hot zone, while Figure F12 illustrates the appearance of several tubes in the cold zone where black powdery material was found on the surface.

The inside surface of the cold inlet header had approximately 1 mil blue oxide on the surface and 1 to 2 mils intergranular penetration beneath the oxide film (Figure F13).

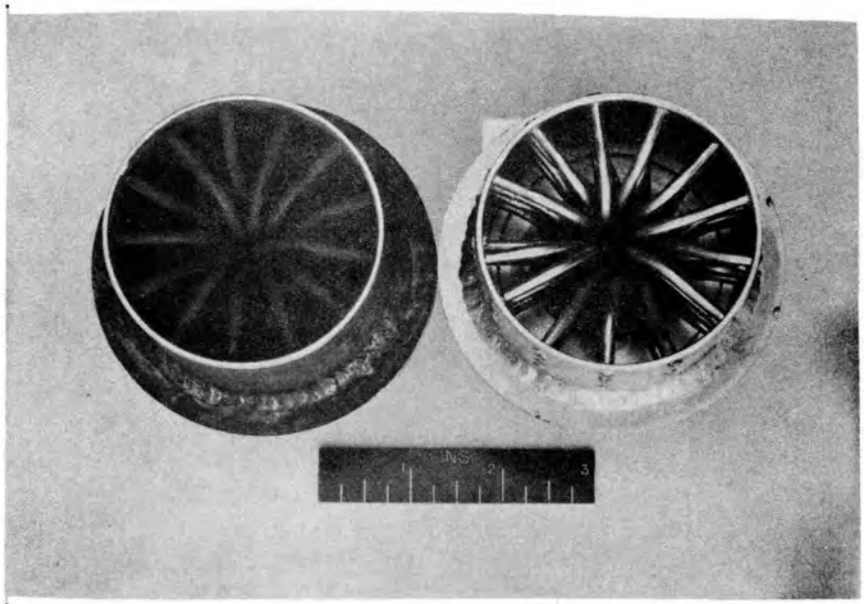

COLD HOT Y-6636

FIGURE F1- HOT AND COLD HEADERS

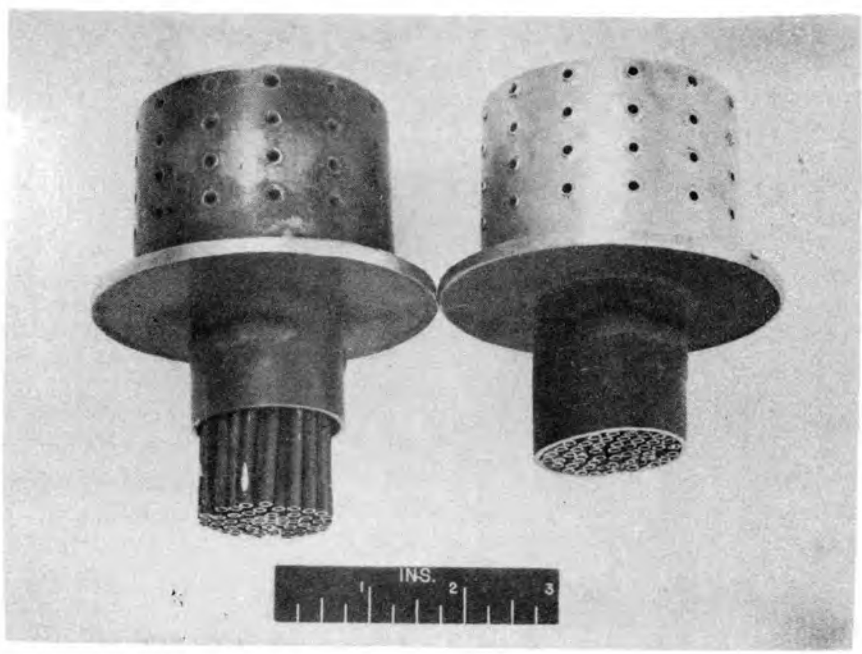

COLD HOT Y-6635

FIGURE F2- HOT AND COLD HEADERS

10 X Y-6677

FIGURE F3- NICROBRAZED TUBE-TO-HEADER

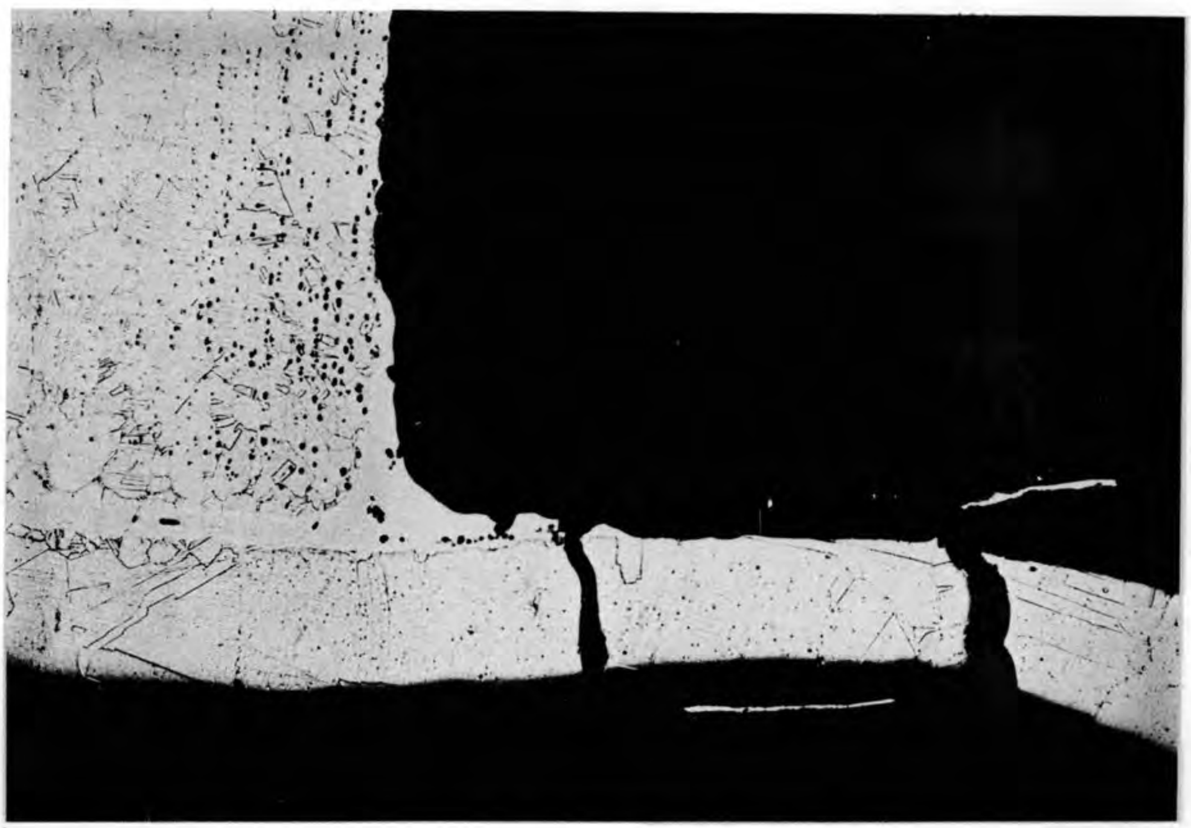

60 X Glyceria Regia Y-6817

FIGURE F4- NICROBRAZED TUBE-TO-HEADER

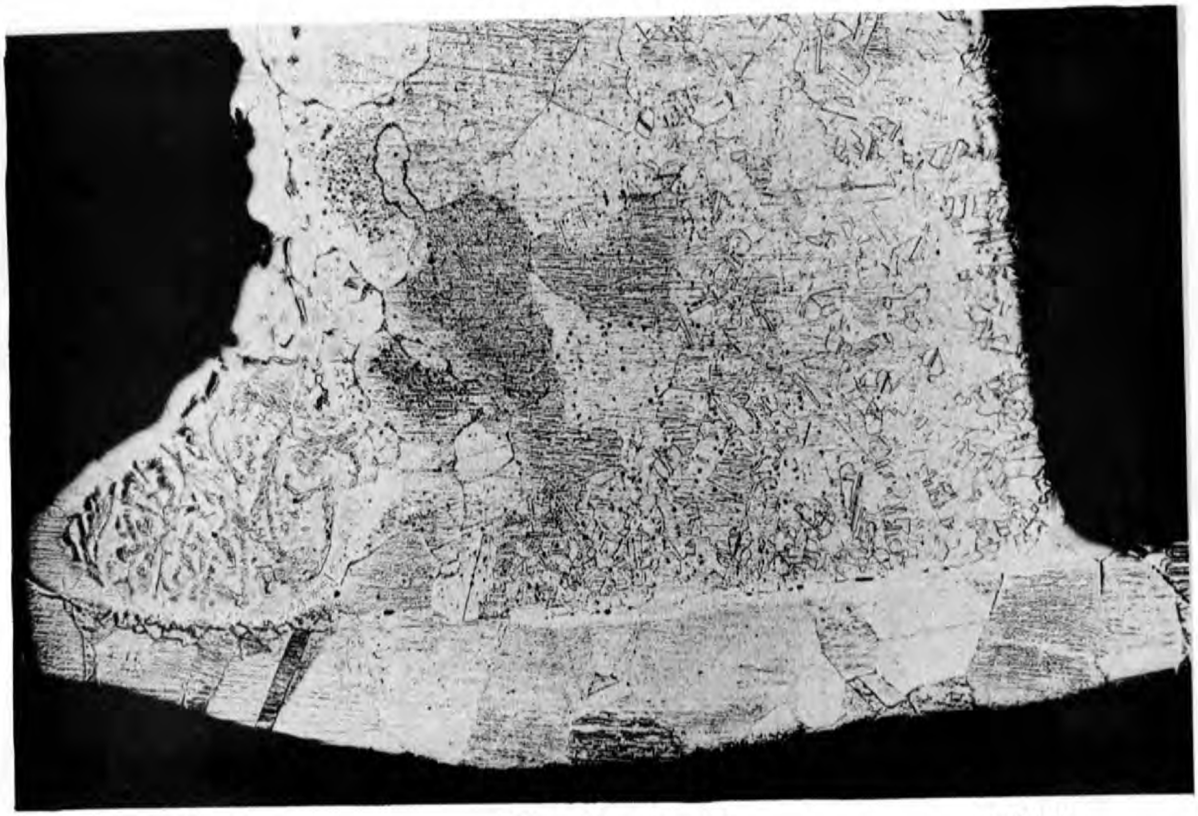

65 X Glyceria Regia Y-6832

FIGURE F5- NICROBRAZED TUBE-TO-HFADER

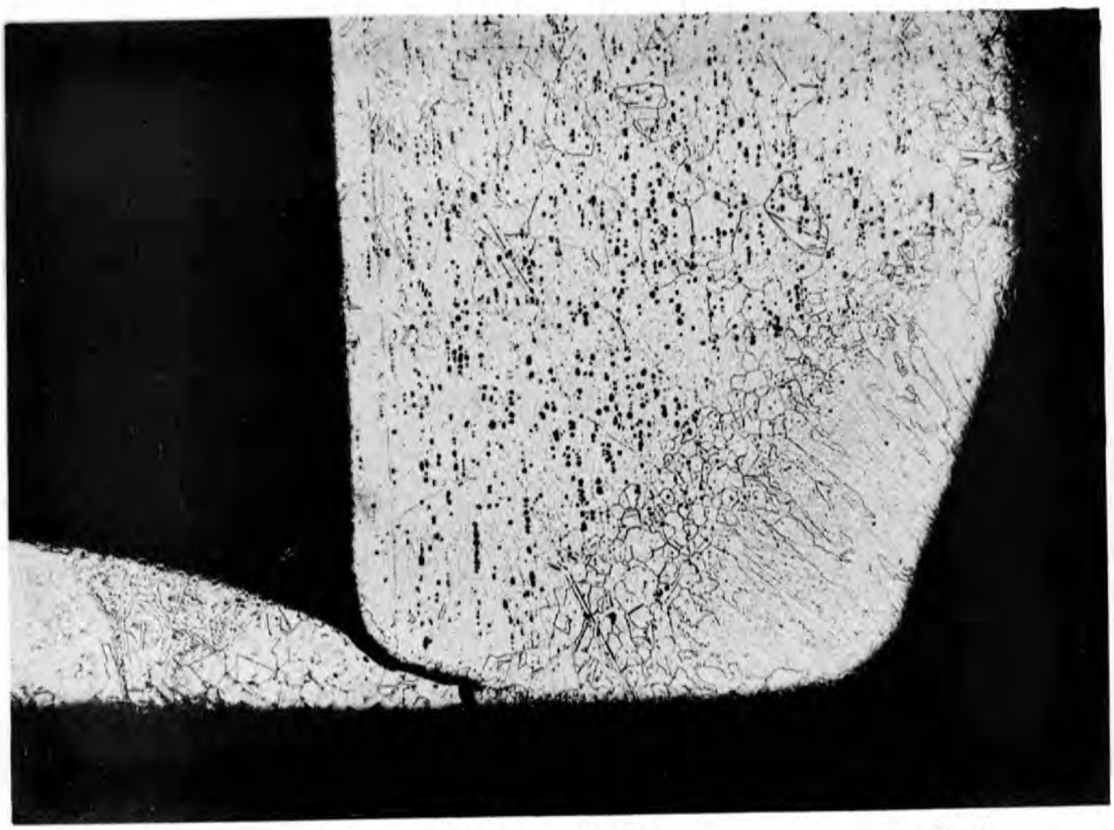

60 X Glyceria Regia Y-6813

FIGURE F6- CONE ARC WELDED 347 SS TUBE-TO-HEADER

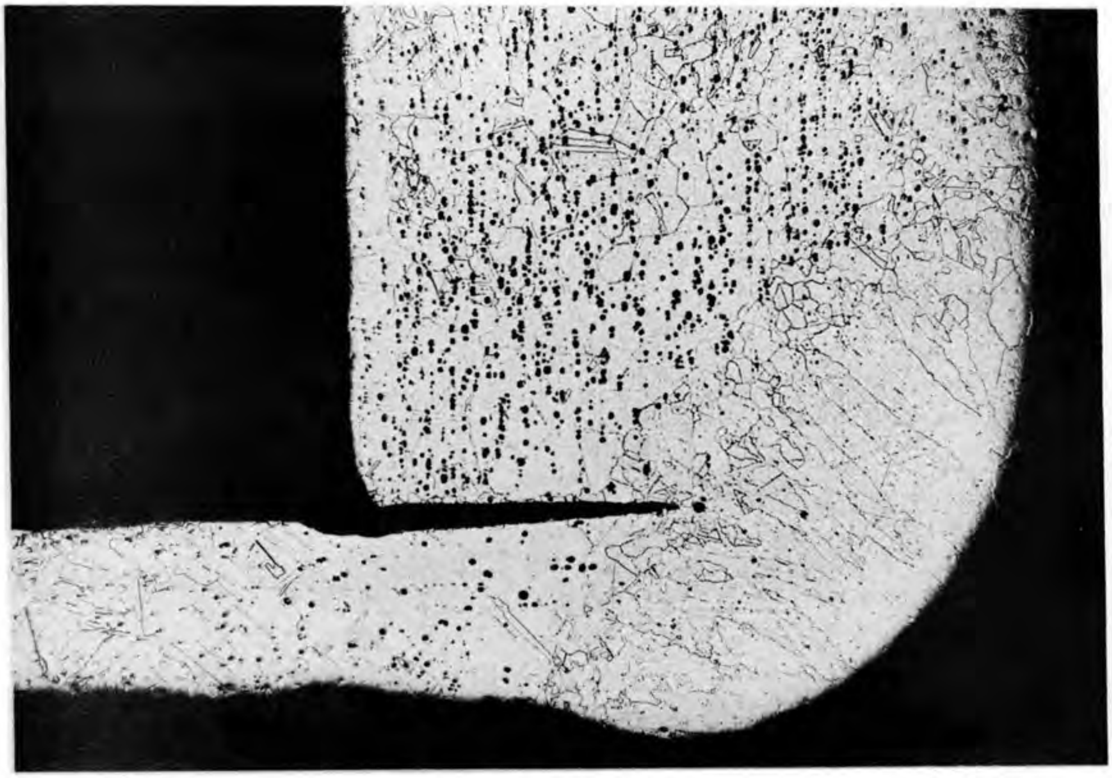

60 X Glyceria Regia Y-6812

FIGURE F7- CONE ARC WELDED 347 SS TUBE-TO-HEADER

80 X Glyceria Regia Y-6873

FIGURE F8- 304 SS TUBE (top) 347 SS TUBE (bottom)

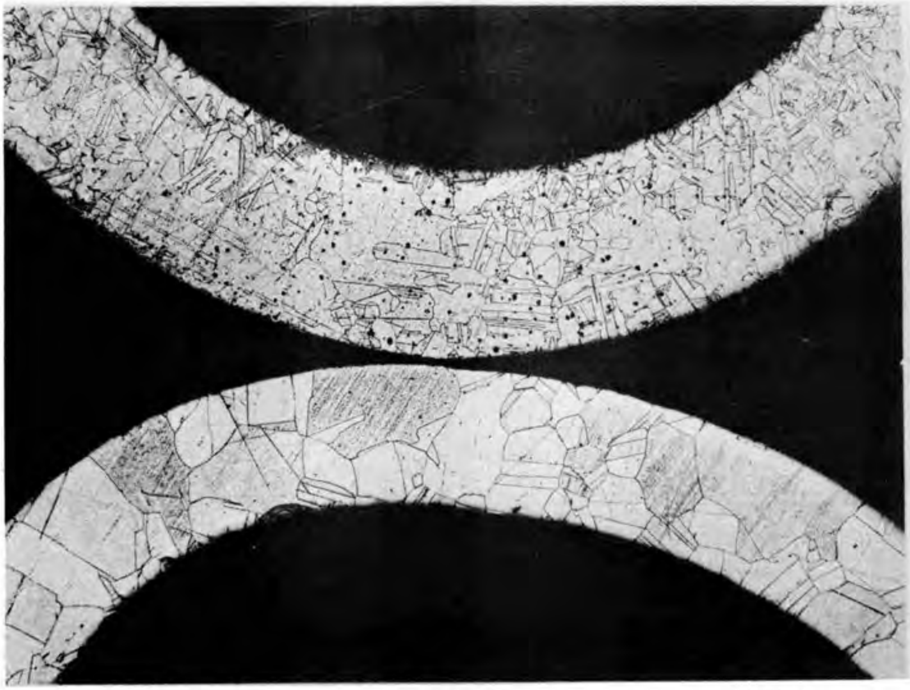

65 X Glyceria Regia Y-6822

FIGURE F9 - 347 SS TUBE (top) 304 SS TUBE (bottom)

125 X Glyceria Regia Y-6831

FIGURE F10- 304 SS TUBE

100 X Glyceria Regia Y-6821

FIGURE F11- 347 SS TUBE

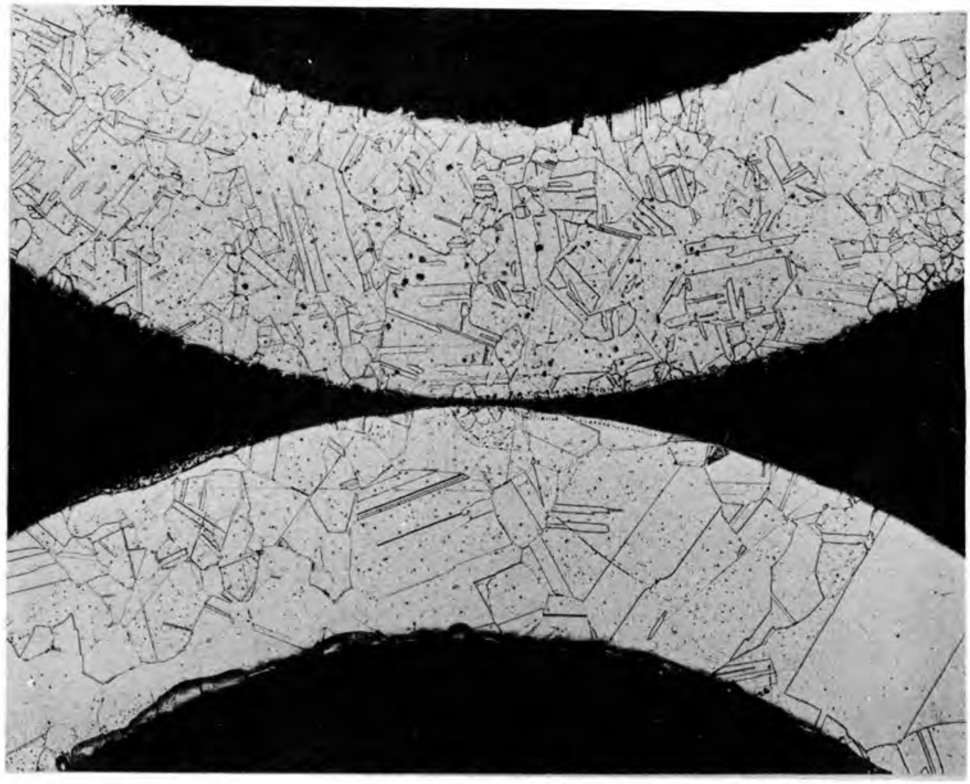

80 X Glyceria Regia Y-6823

FIGURE F12- 347 SS TUBE (top) 304 SS TUBE (bottom)

250 X Glyceria Regia Y-6874

FIGURE F13- SURFACE OF COLD INLET HEADER